Langmuir-Blodgett Deposition of Functionalized AuNRs Towards Multidimensional LSPR Sensing

By

Presley Sarah MacMillan

A Thesis Submitted to
Saint Mary's University, Halifax Nova Scotia
In Partial Fulfillment of the Requirements for the Degree of
Bachelor of Science with Honours in Chemistry

April 2017, Halifax Nova Scotia

Approved: Dr. Christa L. Brosseau
Supervisor
Approved: Prof Mary A.W. Sheppard
Examiner

Date: April 19, 2017

Certification

Langmuir-Blodgett Deposition of Functionalized AuNRs Towards Multidimensional LSPR Sensing

I hereby certify that this thesis was completed by Presley Sarah MacMillan on partial fulfillment for the requirements of the Degree of Bachelor of Science with Honours in Chemistry at Saint Mary's University and I certify that this is truly the original work carried out by Presley Sarah MacMillan.

Thesis Supervisor

Dr. Christa L. Brosseau

Chairperson of the Chemistry Department

Dr. Robert Singer

Dean of Science

Dr. Steven M. Smith

ABSTRACT

Langmuir-Blodgett Deposition of Functionalized AuNRs Towards Multidimensional LSPR Sensing

By: Presley MacMillan

Understanding the surface plasmon resonance properties of gold nanorods (AuNRs) and exploring their sensitivity has attracted much attention due to the potential applications in the biomedical field; including detection of various disease biomarkers through an optimal localized surface plasmon resonance (LSPR).

There are a variety of different techniques available for the synthesis of AuNRs, one of which is the bottom-up approach known as seed-mediated growth. This method introduces a gold seed into a growth solution to obtain gold nanorods of a desired aspect ratio. The goal is to assemble these nanorods at the air-water interface of a Langmuir trough and then compress these nanorods such that a uniform monolayer of well orientated nanorods can be obtained. The goal of this research is to use this monolayer for the synthesis of an LSPR sensor, which will be used for the detection of biomarkers.

April 19, 2017

Acknowledgments

I would like to thank my supervisor Dr. Christa L. Brosseau for accepting me as an honours student and for allowing me to work in her lab. Her assistance has been invaluable in guiding me throughout this project and in helping me learn and progress along the way, ultimately leading me to the completion of this work.

I would like to thank my group members Melanie Davidson, Najwan Al Barghouthi, Dalal Alhatab, Taylor Lynk, Gaius St. Marie, and Osai Clarke. I also want to thank my other friends in the Chemistry Department for their encouragement and support, as well as a special thank you to Reem Karaballi for her valued input and expertise over the past few years. In addition, I would like to thank Dr. Xiang Yang whose technical assistance has been crucial in enabling me to be able to produce scanning electron microscope images of my samples. I would also like to thank my family and friends for their continued encouragement and support.

Finally, I would like to thank all of the Department of Chemistry Faculty and Staff as their knowledge and expertise has greatly assisted me in obtaining a high quality education and in building a solid foundation in the Field of Chemistry upon which I can continue to grow.

Table of Contents

Certification II
ABSTRACT III
Acknowledgments IV
List of Figures: VIII
Chapter 1: Introduction 2
1.1 Introduction: 2
1.2 Localized Surface Plasmon Resonance (LSPR) Biosensors: 3
1.2.1 SPR VS LSPR Sensing: 3
1.2.2 Localized Surface Plasmon Resonance Sensing Limitations: 6
1.3 Review of Nanomaterials: 7
1.3.1 Nanoparticle Introduction: 7
1.3.2 Plasmonic Properties: 9
1.3.2.1 Nanoparticle Size Effects: 9
1.3.2.2 Nanoparticle Shape Effects: 10
1.3.2.3 Sensitivity of Nanomaterials: 11
1.4 Nanorods: 11
1.4.1 Nanorod History: 12
1.4.2 Plasmonic Properties of Gold Nanorods: 12
1.4.3 Sensing Applications: 13
1.5 Langmuir Blodgett Deposition: 15
1.5.1 History of Langmuir Blodgettry: 15
1.5.2 Applications of Langmuir-Blodgett Films - Lipids: 16
1.5.3 Applications to Langmuir-Blodgett Films - Nanomaterials: 18
1.5.3.1 Advantages to Uniform Monolayer of Nanomaterials: 18
1.6 Goal of Thesis: 19
Chapter 2: Theory 20
2.1 Langmuir Monolayers and Langmuir Blodgettry: 20
2.2 Electron Microscopy: 25
2.2.1 Scanning Electron Microscope: 25
2.3 Ultraviolet – Visible Spectroscopy: 30
Chapter 3: Experimental Methodology 31
3.1 Reagents: 31

3.2 Synthesis of Silver Nanomaterials: 31
3.2.1 Silver Nanorods: standard procedure: 31
3.2.2 Silver Nanorods Increased Concentration: 32
3.3 Synthesis of Gold Nanomaterials: 32
3.3.1 Gold Nanorods – CTAB mediated growth: 32
3.3.1.1 Seed Solution: 33
3.3.1.2 Growth Solution: 33
3.3.2 Gold Nanorods – Binary Surfactant Synthesis: 33
3.3.2.1 Seed Solution: 33
3.3.2.2 CTAB and Oleic Acid Growth Solution Synthesis: 34
3.3.2.3 CTAB and Sodium Oleate Growth Solution Synthesis: 35
3.3.3 Isolation of Nanomaterial Colloid: 36
3.4 PEGylation of the Nanorods: 36
3.5 Formation of Nanorod Monolayers: 36
3.5 Instrumentation: 37
3.5.1 Ultraviolet -Visible Spectroscopy: 38
3.5.1.1 Bulk nanorod Sample: 38
3.5.1.2 LSPR Chip Based Sample: 38
3.5.2 Scanning Electron Microscope: 39
3.5.3 Langmuir – Blodgettry: 40
Chapter 4: Results and Discussion 42
4.1 Nanorod Synthesis 42
4.1.1 Silver Nanorods: 42
4.1.2 Gold Nanorods - CTAB mediated Growth: 43
4.1.3 Gold Nanorods – Binary Surfactant Nanorod Growth – Oleic Acid 46
4.1.4 Gold Nanorods – Binary Surfactant Nanorod Growth – Sodium Oleate: 48
4.1.5 Nanorod Synthesis Summary: 51
4.2 Functionalizing the Nanorods: 52
4.2.1: PEGylating the Nanorods: 52
4.2.2 Functionalization Summary: 55
4.3 Langmuir Blodgett Monolayers: 55
4.3.1 PEGylated Nanorods 55
4.3.2 Non-PEGylated Rods: 59
4.3.3 Deposition of PEGylated nanorods in minimal chloroform: 63
4.3.4: Optimizing Langmuir – Blodgett Transfers: 66

4.3.5: LSPR sensor analysis: 68
Chapter 5: Conclusion and Future Work..... 72
Chapter 6: References 73

List of Figures:

Figure 1: Kretschmann configuration for surface plasmon resonance (SPR) sensing.

Figure 2: Example of plasmon resonance λ_{max} wavelength shift.

Figure 3: Lycurgus cup example of the interaction of gold and silver nanoparticles with light.[22]

Figure 4: Gold nanorods of increasing size. [24]

Figure 5: Illustration of transverse and longitudinal modes of a nanorod. Adapted from [45].

Figure 6: Langmuir- Blodgett Isotherm depicting the various states of a lipid monolayer. Reproduced with permission from reference [73]

Figure 7: Cohesive ($\longrightarrow$) and adhesive ($\dashrightarrow$) forces acting on molecules at the gas-liquid interface and molecules in the bulk liquid. Reproduced with permission from reference [73] adapted from. [70]

Figure 8: The Wihelmy plate method to measure the surface tension reproduced with permission from [73]. Adapted from reference [69].

Figure 9: Schematic diagram of a typical SEM. Reproduced with permission from the author [73] Adapted from [82].

Figure 10: Schematic diagram for the production of seed solution #1

Figure 11: Langmuir Blodgett Schematic Diagram Adapted from reference [73]

Figure 12: Attempts at growing silver nanorods.

Figure 13: Gold Nanorod synthesis using CTAB only seed mediated growth method

Figure 14: A subset of the different UV-Vis spectra obtained for the gold nanorod seed mediated growth containing only CTAB, where each color represents a different rod growth solution.

Figure 15: SEM images for gold nanorods CTAB only procedure

Figure 16: UV-Vis spectra obtained for Oleic Acid Binary surfactant nanorod synthesis

Figure 17: Comparison of gold nanorod growth solution color at 2 hours and 23 hours

Figure 18: SEM images of gold nanorods synthesized using CTAB and Oleic Acid. SEM studs prepared using washed colloids. Overlay shows the sample at a distance of 1 μm away.

Figure 19: Binary surfactant method of gold nanorods synthesis using sodium oleate.

Figure 20: SEM image of gold nanorods produced using sodium oleate binary surfactant method

Figure 21: SEM image of gold nanorods produced using sodium oleate binary surfactant method

Figure 22: SEM image of gold nanorods produced using sodium oleate binary surfactant method

Figure 23: SEM image of mPEG-SH nanorods

Figure 24: SEM image of mPEG-SH nanorods

Figure 25: SEM image of mPEG-SH nanorods

Figure 26: Colloidal PEGylated nanorods not dispersed in chloroform.

Figure 27: Colloidal PEGylated nanorods not dispersed in chloroform..

Figure 28: PEG-SH colloidal nanorods dispersed in chloroform added to the air-water interface

Figure 29: PEG-SH nanorods colloid, dispersed in chloroform added to the air-water interface.

Figure 30: PEG-SH nanorods which have been dispersed in chloroform prior to the removal of excess PEG-SH.

Figure 31: PEG-SH nanorods which have been dispersed in chloroform prior to the removal of excess PEG-SH.

Figure 32: Langmuir-Blodgett deposition of PEGylated gold nanorods dispersed in chloroform, manual electrode removal

Figure 33: Langmuir-Blodgett deposition of PEGylated gold nanorods dispersed in chloroform, manual electrode removal

Figure 34: Langmuir-Blodgett deposition of PEGylated gold nanorods dispersed in chloroform, manual electrode removal

Figure 35: Langmuir-Blodgett deposition of PEGylated gold nanorods dispersed in chloroform, manual electrode removal

Figure 36: SEM image of Langmuir-Blodgett transfer 100 mL of bulk mPEG-SH colloid dispersed in 6.6 μL chloroform. Close up image showing a coffee ring.

Figure 37: SEM image of Langmuir-Blodgett transfer 100 mL of bulk mPEG-SH colloid dispersed in 6.6 μL chloroform. Show's the coffee ring effect from a distance

Figure 38: SEM image of Langmuir-Blodgett transfer; 100 mL of bulk mPEG-SH colloid dispersed in 6.6 μL chloroform, showing some multilayer formation.

Figure 39: Optimizing the Langmuir-Blodgett transfer of PEGylated colloidal gold nanorods.

Figure 40: Optimization of the Langmuir-Blodgett transfer of PEGylated colloidal gold nanorods.

Figure 41: Optimizing the Langmuir-Blodgett transfer of PEGylated colloidal gold nanorods, image showing successful increase of surface coverage.

Figure 42: SEM image of the nanorod drop coated LSPR chip.

Figure 43: SEM image of the nanorod drop coated LSPR chip at increased magnification.

Figure 44: SEM image of the nanorod incubated LSPR chip.

Figure 45: SEM image of the nanorod incubated LSPR chip at increased magnification.

Figure 46: Example absorbance spectrum obtained for LSPR chip highlighting the instrument malfunctions.

List of Abbreviations:

APTMS	3-AminopropyltrimethoxysilaneAuNRs
CTAB	Cetyltrimethylammonium bromide
LSPR	Localized Surface Plasmon Resonance
mPEG-SH	Methoxy polyethylene glycol
MPTMS	3-Mercaptopropyltrimethoxysilane
SEM	Scanning Electron Microscopy
SPR	Surface Plasmon Resonance
UV-Vis	Ultraviolet – Visible Spectroscopy
nm	Nanometer
mN/m	Millinewton per meter
μL	Microliter
mL	Milliliter
M	Molar
mM	Millimolar
γ	Surface tension
γ_0	Surface tension of water
Π	Surface pressure

F_p	Weight force
F_a	Archimedes buoyancy force
λ	Wavelength
λ_{max}	Wavelength of maximum absorbance.

Chapter 1: Introduction

1.1 Introduction:

One of the most devastating diseases to afflict mankind is cancer. Simply put, this is because cancer can develop in numerous locations throughout the body, each resulting from a different cause and each with its own signs and symptoms. According to the Canadian Cancer Society, one-third of all people diagnosed with cancer will die. On average 555 Canadians are diagnosed daily, and a further 216 die each day as a result of cancer.[1,2]

8-oxo-2'-deoxyguanosine is an oxidized derivative of the molecule deoxyguanosine. Measuring the amount of 8-oxo-2'-deoxyguanosine in a cell is one way to measure the amount of DNA oxidation that has taken place.[3,4] This molecule has been well studied, and it has been determined that the levels of 8-oxo-2'-deoxyguanosine can be used as a way to predict the formation of cancer, as oxidative damage can be a precursor to DNA mutations.[3,4] It is clearly apparent and imperative that a quick and easy method of detecting the presence of this molecule and others like it be developed so that treatment programs can be started as soon as possible. Currently it takes days to weeks, and in extreme cases months to obtain a clear cancer diagnosis.[5] The aim of this project is to develop a "proof of concept" for the formation of point-of-care cancer diagnostics using a plasmonic resonator. This will be accomplished by developing a means of detecting the cancer biomarker 8-oxo-2'-deoxyguanosine using fabricated localized surface plasmon resonance (LSPR) biosensors in which the plasmonic properties of gold nanorods (AuNRs)

will be optimized and a change in the maximum extinction of the AuNRs will be used to monitor the concentration of 8-oxo-2'-deoxyguanosine present in a sample.

1.2 Localized Surface Plasmon Resonance (LSPR) Biosensors:

1.2.1 SPR VS LSPR Sensing:

Surface plasmons have been studied for years by chemists, physicists, biologists and material scientists, due to their widespread applicability in many areas of progressive development including electronics, medicine and optical sensing[6]. Surface plasmon resonance (SPR) gained prominent attention between 1982 and 1983 when they were used for gas detection and biosensing as demonstrated by Nylander and Liedberg[7,8]. The excitation of surface plasmons was discovered by Kretschmann and Otto in the late 1960s.[9,10] Kretschmann became influential in the production of SPR technologies, and today the majority of SPR sensors use a standard set-up known as the Kretschmann configuration, which is shown below in Figure 1. In this set-up a light source is shone through a prism towards an SPR chip, where it is reflected at a certain incident angle towards a detector. At this incident angle which is referred to as the resonance angle, the light from the source is absorbed by the electrons in the metal SPR chip, causing the electrons to resonate. These resonating electrons are the source of the SPR name and are known as surface plasmons. The process of electrons absorbing light results in a net decrease in the intensity of light that is reflected back to the detector. This intensity decrease is observed as a decrease in the SPR intensity curve or as a large increase in intensity when monitoring absorbance. Both the shape and the location of this absorbance change can be used to monitor binding of the surrounding environment to the SPR chip. To accomplish this intensity change, a probe molecule is immobilized onto the chip and

suspended into a solution containing an analyte of interest. As molecular binding takes place, a change in the incident angle is measured and a shift in the absorbance is obtained. This peak shift can be used to provide information regarding the concentration of an analyte within the solution. This technology can also be used to provide real time analysis of a solution by monitoring the change in SPR absorbance, allowing for the kinetics of the reaction to be studied with ease.

While SPR technology is a useful method of sensing, it is limited by sensitivity and resolution. It also requires the use of expensive instrumentation and sample accessories / consumables.[11] Additionally, because SPR monitors the refractive index of a bulk solution, the results are highly influenced by environmental factors such as temperature and viscosity changes.[12] It is in these areas however that LSPR sensors excel or have the ability to excel, as they continue to be studied and optimized.

Localized surface plasmon resonance sensors rely on a transduction method analogous to SPR sensors.[13] Originally it was noted that the refractive index sensitivity of the SPR sensors was four (4) orders of magnitude lower than that of LSPR sensors[14,15]. This discovery lead to the conclusion by many within this field that LSPR sensors would be less sensitive than SPR sensors of the same order of magnitude. This was however later proven to be incorrect as it was found that the two are actually very comparable in their sensitivity levels, as the LSPR nanosensor has a very short electromagnetic field decay length which is able to increase the sensitivity of the sensor. LSPR sensors are comprised of nanoscale metals; most commonly these nanoscale metals are spherical. However, it has been found that the shape, size and composition of the metals greatly change the electromagnetic decay length.

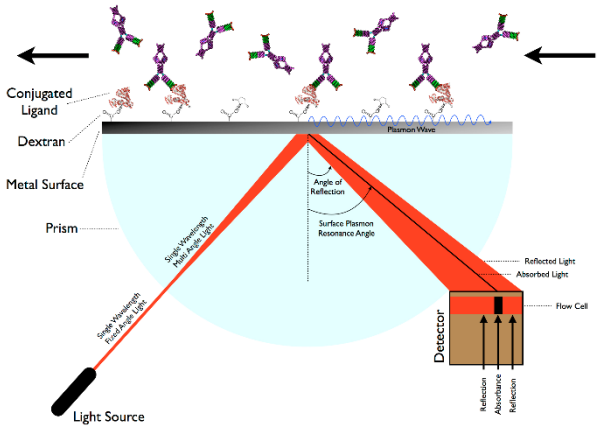

Figure 1: Kretschmann configuration for surface plasmon resonance (SPR) sensing.[16]

To summarize, a localized surface plasmon resonance (LSPR) is an optical phenomenon which is generated by the interaction between light waves and the conductive nanoparticles. A light wave becomes trapped by the nanoparticles which are smaller than the wavelength of the incident light, causing an interaction between the light and the surface electrons which are located in the conduction band.[6] This interaction produces localized plasmon oscillations which have resonance frequencies that are tuneable based upon the composition, size, geometry dielectric environment, and the separation between the nanomaterials.[6]

With emerging advancements in the field of nanotechnology an interest in the plasmonic properties of nanomaterials has arisen. The most common materials used to produce nanoparticles are noble metals such as gold and silver as a result of their favorable plasmonic properties. The energy level of their d-d transitions produces an LSPR which lies in the visible region of the electromagnetic spectrum. For this project, gold is preferred because of its biocompatibility, and the ease with which nanostructures can be synthesized.

Due to the short electromagnetic decay length of an LSPR sensor of ~5-15nm[13], a high reliance is placed on molecular interactions happening on or very near the surface of the LSPR chip. This in effect means that the refractive index of a bulk solution is negligible, as only the change in refractive index near the surface of the LSPR chip is monitored. Consequently, LSPR sensors do not require temperature control as the change in refractive index due to temperature has a negligible effect in the small region near the chips surface.[13]

An additional benefit of using an LSPR based sensor over a traditional SPR sensor is the cost involved. Typically the instrumentation required for a SPR sensor ranges from $150,000 – $300,000[13] or higher. To obtain comparable results with an LSPR sensor, the typical cost ranges from $5000 – $10,000.[17] These advantages suggest that LSPR sensing could be useful for POC analysis.

1.2.2 Localized Surface Plasmon Resonance Sensing Limitations:

A strong interest in studying localized surface plasmon resonances began in the early 1980's concurrently with that of surface enhanced Raman spectroscopy[18]. Since this time LSPR has been studied in depth and it has been determined that while the sensitivity of LSPR sensors are comparable to SPR sensors, this is still one of the major limitations to using this method. Recent simulations[19,20] have suggested that the refractive index sensitivity for these sensors increases linearly as the LSPR frequency of the materials shifts from the blue region of the visible spectrum to the longer red wavelengths. This shift in wavelength can be achieved by increasing the size of the nanostructures and by incorporating asymmetry into the nanostructures as discussed in Section 1.4. Currently the limitation for this technology lies in its ability to produce easily measured LSPR wavelength shifts in the presence of the target analyte. In most instances, especially when

the analyte in question is a small molecule, the change in wavelength shift is less than 1 nm. This introduces ambiguity into the possible cause of the shift, along with a requirement for the use of expensive high resolution equipment.[21] Thus a variety of methods for improving this technique have been proposed along with increased nanomaterial size, shape, and anisotropic. These range from techniques more focused on biological sensing including enzyme amplification and plasmonic coupling as a means of increasing the shift in the plasmon resonance.

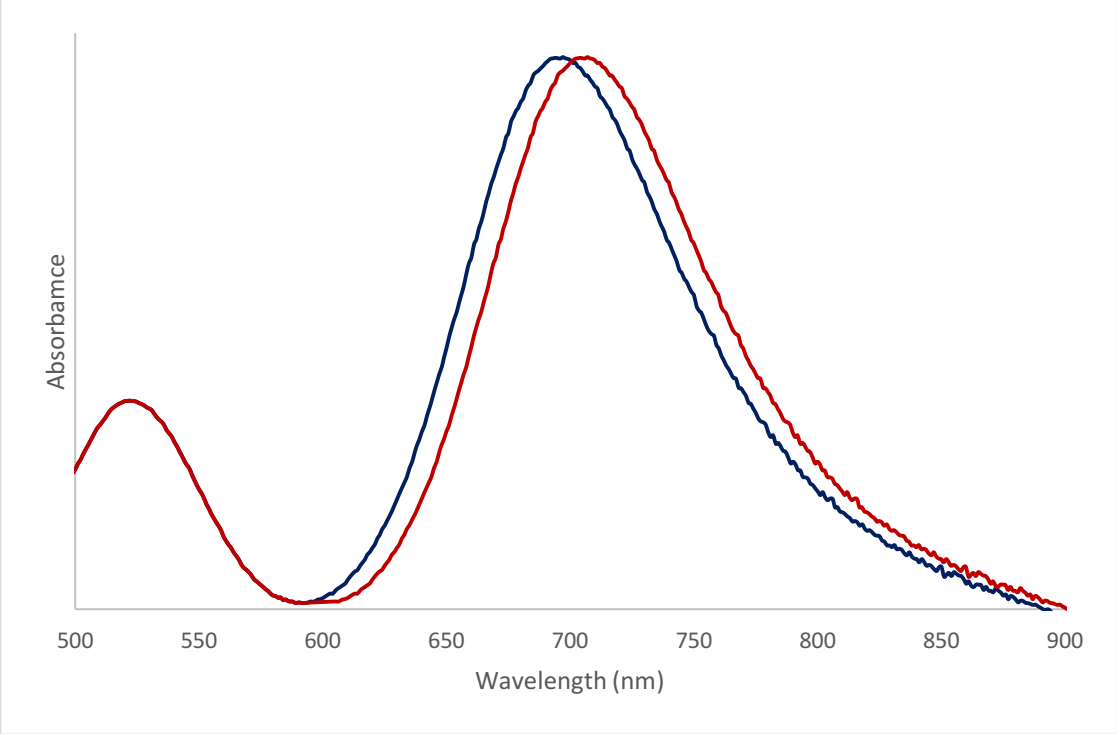

Figure 2: Example of plasmon resonance λ_{max} wavelength shift.

1.3 Review of Nanomaterials:

1.3.1 Nanoparticle Introduction:

Plasmon nanoparticles are primarily made from the coinage metals, primarily gold and silver. Nanoscale metals have been incorporated into everyday things for centuries due

to the interesting ways in which they interact with light. Nanoparticles have been used as a way of introducing colors into relatively common items long before it was discovered that nanoparticles were in fact the root cause of the colors. Arguably the most famous example of this from history was the Lycurgus Cup, which can be seen in Figure 3. Other common examples include the use of nanoparticles in the stained glass found in church windows which originate as early as the 12th century. The interaction of nanomaterials with light is a highly variable property which is greatly influenced by the shape and size of the particles.

Figure 3: Lycurgus cup example of the interaction of gold and silver nanoparticles with light.[22]

Recently the useful properties that nanoparticles possess have been explored in more depth and have brought the study of them to the forefront of research. It has been discovered that the interactions nanoscale materials have with light is able to be utilized and measured making them very valuable in sensing applications. Furthermore, it is widely recognized that nanoparticle suspensions are extremely stable. While silver nanoparticles have a relatively short shelf-life due to oxidation of the particles, gold nanoparticle

suspensions can potentially remain stable indefinitely. A great example of this is the first documented colloidal gold suspension prepared by Michael Faraday in 1846 which is currently on display in the Faraday Museum in the United Kingdom.[23]

1.3.2 Plasmonic Properties:

Free conduction electrons in metal nanoparticles are capable of interacting with incident light waves. The most notable of these includes gold, silver and platinum nanoparticles. In the presence of a light wave of the right energy, a phenomenon occurs in which the electrons in the outer shell of the metal collectively oscillate and are able to produce what is known as a surface plasmon. The energy at which the electrons are capable of producing this plasmon are unique to some specific properties of the nanoparticle. Most notably is the type of metal, followed by the size of the particle.

1.3.2.1 Nanoparticle Size Effects:

The size of a nanoparticle is a controllable feature which is able to tune the wavelength at which the particle absorbs and interacts with a wavelength of light. A general trend for the tunability of nanoparticles is that as the size of the particle increases the wavelength of maximum absorbance redshifts. This is visually apparent when looking at solutions of nanoparticles of various sizes, as the color of the solution changes depending upon the size of the particle, similar to that shown in Figure 4. The characteristic maximum absorbance obtained for a nanoparticle of a specific size can play a key role in the use of nanoparticles as a sensing mechanism. By monitoring changes in this peak when various analytes are present, the interaction of nanoparticles can be monitored.

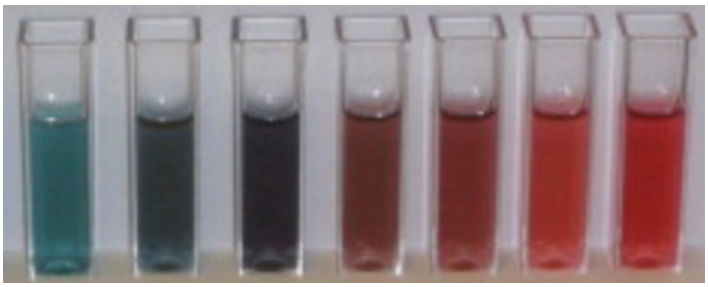

Figure 4: Gold nanorods of increasing size.[24]

1.3.2.2 Nanoparticle Shape Effects:

While nanoparticles of increasing size are able to interact with light and various mediums in unique ways, changes in the shape of the nano-sized particles can also have a dramatic impact on the way in which the particles behave. The term *nanoparticle* is widely used to refer to spherical shaped particles. While in the past spherical particles have been by far the most common shape used in most nanomaterial applications, it is by no means representative of the number of particle shapes possible. Nanomaterials can be produced in a wide variety of shapes which are generally defined and classified in one of two ways. Isotropic (spherical) or anisotropic (non-spherical).[25] Isotropic particles have quantum confinement in all three dimensions and as a result are considered zero dimensional or 0D nanomaterials. Anisotropic is used to encompass all other shapes which can be one, two or three dimensional, referring to the amount of confinement in the shape. Arguably the most common nanoscale shapes for the 1D and 2D materials are nanorods and nanosheets respectively. Biologically the shape of the nanomaterial can greatly affect the uptake and/or the rate of drug delivery. It can also affect the specific proteins which can interact with the particle.[26] The shape of a nanoparticle has been shown in some studies to affect the way in which the particle can interact with the cell membrane.[27] Anisotropic shapes are gaining interest in the field of nanomedicine due the large surface area and the ability to provide

good binding arrangements for drugs, highlighting the potential for use in sustained drug delivery.[26]

1.3.2.3 Sensitivity of Nanomaterials:

As outlined earlier, nanomaterials have a variety of different characteristics that can be used to define them. For example, properties such as the size and the shape of the particles can be directly related to the sensitivity associated with a variety of applications. When referring to plasmonic nanoparticles sensitivity usually refers to the sensitivity of the plasmonic response associated with the materials.

1.4 Nanorods:

Nanorods are a one dimensional nanostructure which have sparked increased interest because of the attractive properties they exhibit. Nanorods have a plasmon-resonant absorption and scattering in the near- Infrared (NIR) region of the spectrum[28]. This makes them attractive as probes for *in vitro* and *in vivo* imaging.[28] Due to the efficient absorption in the NIR region, gold nanorods are able to permit photons to penetrate biological tissue with a relativity high transmittivity.[28] Gold nanorods (GNRs) are highly tunable as a function of their aspect ratio, in which the optical resonances can be tuned towards either the visible or NIR wavelengths. This property increases the number of applications in which GNRs can be utilized. Gold nanorods can be synthesized utilizing a variety of methods. Currently one of the most cost effective methods for the production of GNRs is the seed mediated growth method.[29,30] However, other methods such as the template method or electrochemical methods are among others that are frequently used[31].

1.4.1 Nanorod History:

Nanorods and nanowires were among the first nanoshapes other than spheres to be developed. The development of these new shapes spurred an increased interest in anisotropic shapes in general. One of the first demonstrated examples of these shapes was in the late 1990s when the electro-templated and photochemical synthesis of gold nanorods was released. Shortly thereafter at the turn of the 21st century, a number of seeded growth synthetic methods were developed and reported on.[32-36] Thereafter, slight variations in the synthesis procedures further advanced research, and made it relatively easy to develop nanorods of a desired aspect ratio. In 2003 interest in nanorods exploded with the introduction of one-step silver assisted seeded growth nanorod production.[37] Even more recently, these techniques have been optimized and rods can now be reliably synthesized with a desired aspect ratio.[37]

1.4.2 Plasmonic Properties of Gold Nanorods:

Gold nanorods have unique plasmonic properties which are not exhibited by their spherical counterparts. The plasmonic response of gold nanorods in the visible –NIR region is characterized by two peaks in the absorption (extinction) spectra. These peaks arise as a result of the rod shape, and they are referred to as the longitudinal and transverse modes. The peaks correspond directly to the 1D rod shape, in which the transverse peak is a result of the shorter side of the rod, and the longitudinal peak is a result of the longer side. These two plasmon resonance modes make the rods significantly more sensitive to the surrounding dielectric environment. The plasmon resonance is an optical phenomenon that occurs at the surface of a nanoparticle of the appropriate size. The nanoparticle interacts with incident photons and is capable of inducing an oscillation of the conduction band

electrons contained at the surface of the particle.[37] Gold nanoparticles varying in size from approximately 3 – 200 nm are capable of promoting a plasmon resonance which is highly dependent on the radius of the nanoparticle. In contrast the plasmon resonance of a nanorod is affected most strongly by the aspect ratio of the nanorod.[37-41]

The length of nanorods also plays a key role in the plasmonic behaviour that is exhibited by the rods. A comparison of the optical properties exhibited by nanorods of the same aspect ratio was completed.[39,40] In this study rods with an aspect ratio of ~4 and with a length of ~25 nm were compared to rods of 60 nm with the same approximate aspect ratio.[39,40] This study was able to confirm that the extinction coefficient of larger rods is more sensitive than that of the smaller rods which was a direct implication of the their relative scattering efficiency.[40] This realization is important in potential imaging applications, suggesting that the larger rods would be more effective in these applications whereas the smaller rods may be more efficient in photothermal applications.[37-44]

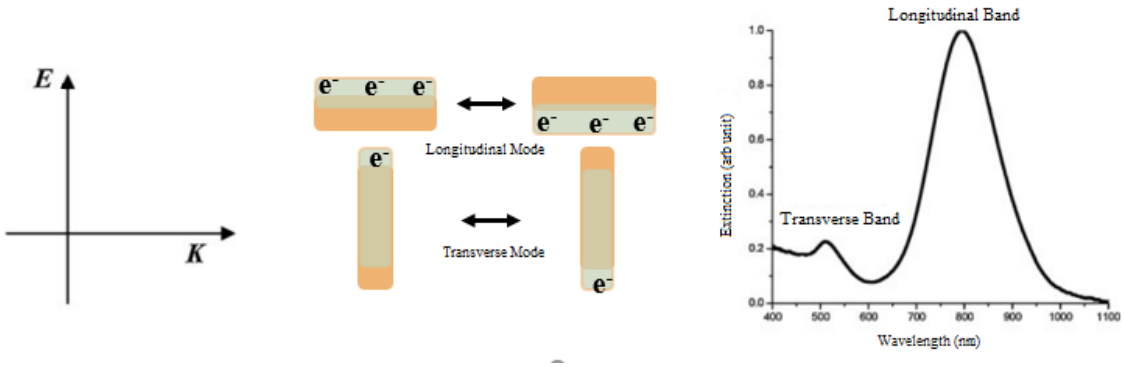

Figure 5: Illustration of transverse and longitudinal modes of a nanorod. Adapted from [45].

1.4.3 Sensing Applications:

Due to the unique properties that nanorods exhibit, such as the two resonance modes which can be monitored using visible spectrophotometry, they are promising tools

for sensing applications. There are currently a number of common sensors which make use of plasmonics. These sensors can be classified in a variety of ways including colorimetric sensors, surface plasmon resonance sensors (SPR), sensors which make use of the Rayleigh scattering, and label-free sensors which rely on changes in refractive index.[43] While each type of sensor has its own unique advantages and disadvantages, the sensing applications which will be highlighted are those pertaining to the LSPR based sensors, primarily those which are chip based.

SPR sensors are highly sensitive to the refractive index change in the dielectric environment, i.e. highly sensitive towards the medium surrounding the metal film of the sensor. Standard SPR sensors are based on the attenuated total reflection (ATR) configurations.[43,44] More recently enhancements in the sensitivity of these sensors has been obtained by utilizing localized surface plasmons (LSP) or localized surface plasmon resonance (LSPR). The addition of LSP allows for the stronger optical coupling of incident light into the resonance and the momentum of the surface plasmon.[45-53] LSPR sensors have been successfully synthesized using nanoparticles. However, by building a nanorod based sensor it is possible to take full advantage of the nanorods resonant properties, which subsequently increases the sensitivity of the sensor.

Chip based LSPR sensors are an extremely common form of LSPR sensor. This type of sensor is normally fabricated by immobilizing nanoparticles and/or nanorods on the surface of a flat and transparent substrate such as glass coverslip or glass slide. [54] Two main methods are used to do this when the nanorods are grown using a method such as the seed mediated method; the electrostatic force method and a self-assembled monolayer (SAM) method.[54] The electrostatic method suffers from poor stability and poor uniformity.

This limits its application and as a result the SAM based method has become more common.[54] This method usually first involves modifying the substrate in an alkylsilane solution such as 3-aminopropyltrimethoxysilane (APTMS) or 3-mercaptopropyltrimethoxysilane (MPTMS), which forms an amine-terminated silane SAM on the surface of the substrate. The substrate is then incubated in the solution of gold nanorods to form a monolayer of gold nanorods on the surface of the substrate. Once completed, the gold nanorods can be further functionalized as necessary in order to make the sensor chip useful in a wide range of applications.[54] An effective method for measuring the LSPR is through the use of UV-Vis spectrophotometry. Using UV-Vis spectrophotometry the change in wavelength of maximum absorbance (λ_{max}) can be monitored. Due to the sensitivity of the LSPR chip to the refractive index of the surrounding material, a wavelength shift has the potential to indicate the presence of the analyte of interest. In some cases, this can be extended to include determination of the concentration of the analyte of interest present in the sample being monitored. The simplicity of the instrumentation used to monitor these changes (a relatively standard spectrophotometer), means that not only is it an effective technique, it is also a relatively fast and inexpensive method of analysis which has promising potential for use as a point of care diagnostic technique.

1.5 Langmuir Blodgett Deposition:

1.5.1 History of Langmuir Blodgettry:

The Langmuir Blodgett deposition of monomolecular films can be thought of as the result of a linear progression which began with Benjamin Franklin in approximately 1770 with his experiments and observations regarding the spreading of oil on the surface

of water in a pond. After Franklin's observations in the late 18th century it wasn't again until the 19th century that Rayleigh was able to quantify the observations and calculate the thickness of the oil which had covered the pond. The work of Agnes Pockels also contributed to what is known as the Langmuir Blodgett technique when she noted that the area of the films created can be controlled using barriers, and that the surface pressure increases as the films are compressed.[56] This work directly influenced Langmuir and he expanded upon this technique by developing what is known as the Langmuir trough. With the use of this trough Langmuir was able to determine the chain length of the molecules he added to the trough while also being able to accurately describe their orientation.[57]

With the help of his assistant Katharine Blodgett, Langmuir was able to enhance his studies of surface chemistry and floating monolayers to learn about the nature of intermolecular forces; it was for this work that he was awarded the Nobel Prize in chemistry in 1932. The ideas and techniques that were developed by Langmuir and Blodgett in the first half of the 20th century are still used with some alterations for studying monomolecular films. Langmuir and Blodgett together were able to refine the methods for transferring floating monolayers onto solid supports thus developing the method commonly referred to as the Langmuir-Blodgett method.[57]

1.5.2 Applications of Langmuir-Blodgett Films - Lipids:

Langmuir-Blodgett films are appealing because they provide control over a variety of parameters which directly influence the structure of the film including precise control of monolayer thickness.[57] Langmuir monolayers are comprised of a substance that is insoluble in water but is soluble in a volatile substance such as chloroform. This allows for sufficient spreading of the substance along the surface of the water. Most commonly the

Langmuir- Blodgett method is used to compress lipids or other like molecules (amphiphiles) in which there is a “head” and “tail” group. The “head” is hydrophilic and typically contains a group in which a strong diploe moment is present and the “tail” contains a hydrophobic group.[57] The molecules orientate themselves at the surface with the head group along the surface of the water and the tail group pointing upward. This monolayer can then be compressed and monitored by measuring the surface pressure of the layer. During the compression the lipids orient themselves in such a way that they mimic the states of matter as shown in Figure 6.

Prior to compression the lipids have no order and mimic the gaseous phase of matter. As compression begins and surface pressure increases the lipids slowly become ordered mimicking the way in which molecules behave in a liquid. When the monolayer is compressed tightly the molecules all align and behave like molecules in a solid, until compression goes too far and the monolayer collapses. The monolayer can be compressed to the desired level of order and then transferred to a solid substrate. The study of such films can be used to provide valuable information about biological membranes, as many lipids are main components in membranes. Some of the most common applications of the Langmuir – Blodgett method include producing cell membrane model structures, studying drug delivery and behavior, as well as the interactions of proteins. Langmuir – Blodgett deposition has also been used to study polymerization, surface adsorption, along with optical, electrical and structural properties to name just a few.[58]

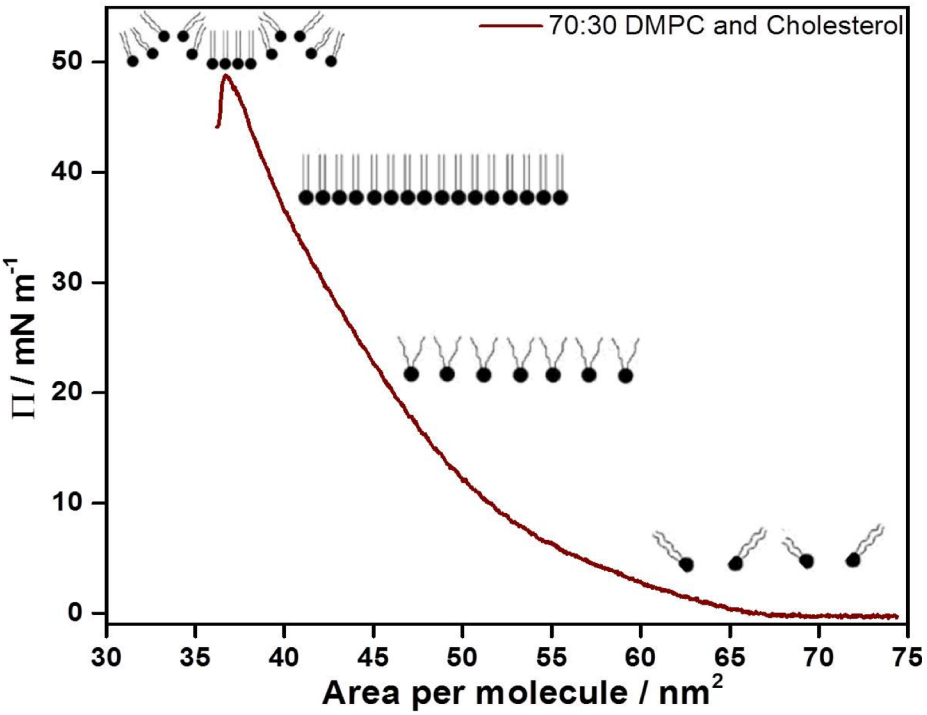

Figure 6: Langmuir- Blodgett Isotherm depicting the various states of a lipid monolayer. Reproduced with permission from reference [73]

1.5.3 Applications to Langmuir-Blodgett Films - Nanomaterials:

In recent years, Langmuir-Blodgett depositions have been extended for use with nanomaterials. While the standard Langmuir-Blodgett procedure is designed for use with lipids, increasing interest in nanomaterials has led to the technique being used in an attempt to produce ordered monolayers of nanomaterials. Langmuir-Blodgett with incorporated nanomaterials have been produced primarily over the past 15 years.[59-64]

1.5.3.1 Advantages to Uniform Monolayer of Nanomaterials:

A uniform monolayer of nanorods has many potential benefits; as outlined in previous sections the LSPR of nanorods is more sensitive than that of nanoparticles and more easily tuned. In an ordered array the LSPR properties of the nanorods should be further enhanced similar to the way in which local hot spots of strongly coupled

nanoparticles are orders of magnitude higher than those of single nanoparticles.[65] This means that an ordered array should have enhanced sensing properties which can be practically beneficial for Raman and surface enhanced Raman spectroscopy.[66]

1.6 Goal of Thesis:

This thesis explores the preparation of arrays of gold nanorods for use as an LSPR sensing platform for the detection of biomarkers. A proof of concept LSPR sensor platform will be developed by applying a uniform monolayer of gold nanorods to a substrate using the Langmuir-Blodgett method followed by further functionalization with a DNA probe of interest. The first step was to successfully synthesize reliable nearly monodispersed gold nanorods, followed by a successful transfer of these rods to the air-water interface using the Langmuir – Blodgett trough, and subsequent successful transfer onto a solid substrate. Taking this one step further the next step was to determine if a glass cover slip would be a successful substrate for monitoring the change in LSPR.

Chapter 2: Theory

2.1 Langmuir Monolayers and Langmuir Blodgettry:

To obtain a compact monolayer of lipids using the Langmuir – Blodgett technique, some basic thermodynamic principles need to be studied. These same principles apply for the use of Langmuir Blodgett with nanomaterials. Primarily, molecules at the air-water interface will orient themselves in such a way that thermodynamic equilibrium is reached to minimize their free energy.[69] With reference to thermodynamics, free energy is defined as the energy required for a system to do work. While suspended at the air-water interface the molecules are subject to a net inward force. This is due to the molecules being surrounded by fewer molecules than would have been present in the bulk solution as shown in Figure 7. At the interface, the molecules are not subject to forces of attraction in all directions, leading to a force imbalance.[70] The forces between molecules (intermolecular

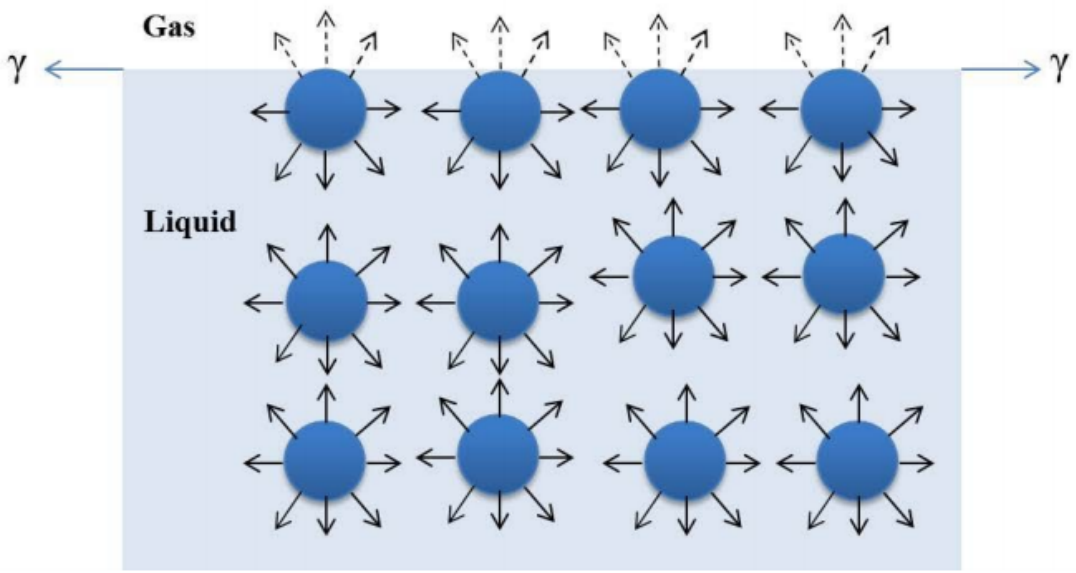

Figure 7: Cohesive (⟶) and adhesive (⇢) forces acting on molecules at the gas-liquid interface and molecules in the bulk liquid. Reproduced with permission from reference [73] adapted from. [70]

forces) that occur between different substances are referred to as the cohesive and adhesive forces.[71] At the air-water interface monolayer chains are subject to high cohesive interactions.[72] Cohesive forces keep the phases separate due to the tendency for a substance to hold itself together.[3] While a molecule at any interface is subject to both cohesive and adhesive forces, at the air-water interface the cohesive forces are much stronger, causing the net force imbalance and resulting surface tension.[71] This can be defined as the energy needed to increase the surface area of a liquid.[73]

The force acting on the molecules at the gas-liquid interface is referred to as the surface tension (γ). This is one of the standard physical values used to characterize liquid phases. Surface tension is the result of short-range intermolecular forces; these include Van der Waals forces and hydrogen bonding.[70,73] Surface tension can be more easily understood when compared with surface pressure, Π. Surface pressure can be explained by the compression of molecules using the barriers of the Langmuir Blodgett at the air-water interface.[73] As the barriers compress the surface pressure increases as a result of the molecules being forced into closer proximity with one another. Consequently, the work required to move the barrier can be expressed as the product of the distance travelled by the barrier (Δx), the length (l) of the barrier and the surface pressure (Π),[73] shown in equation 1:

$$w = \Delta x * l * \Pi \qquad (1)$$

A change in surface energy results as a result of the molecules being compressed at the interface. In Langmuir-Blodgett monolayer experiments reference to surface pressure

measurements rather than surface tension measurements are common.[69,73,74] The surface pressure can be expressed as the difference between the surface tension of the water (subphase), γ_o and the surface tension of the monolayer, γ shown in equation 2:

$$\Pi = \gamma_o - \gamma \quad (2)$$

Surface tension is also expressed as the force per length acting on the surface, this translates into an SI unit of mN m^{-1}. Various methods are used to obtain the surface tension

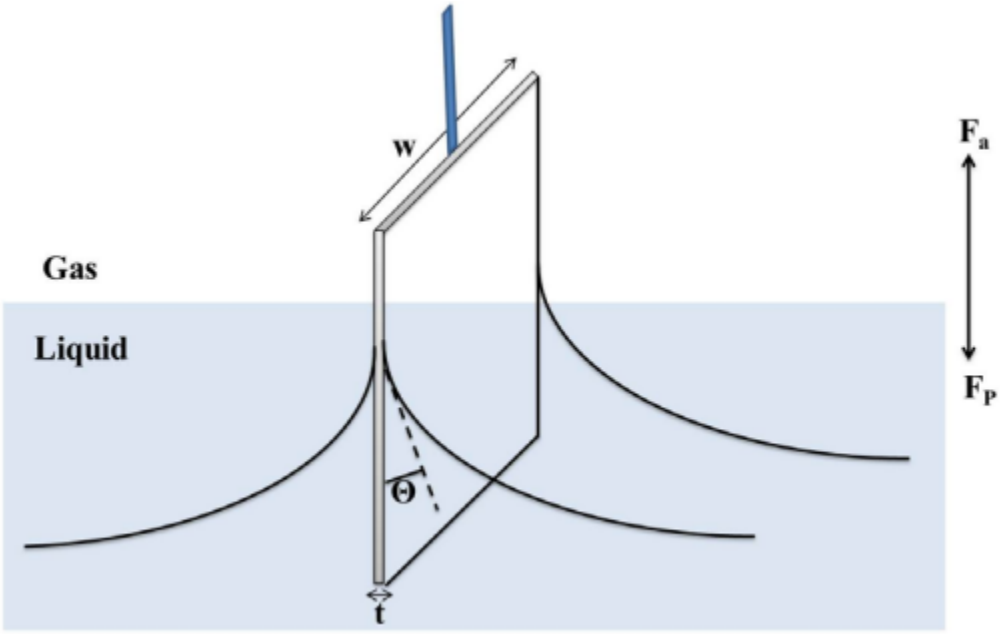

Figure 8: The Wihelmy plate method to measure the surface tension reproduced with permission from [73]. Adapted from reference [69].

of a monolayer as it is compressed, the most common of which is the Wilhelmy plate method. [69,73,74] This method uses a flat plate to measure the different forces occurring at the surface of the liquid, and works by dipping a flat plate into the surface of the liquid.[69] This is connected to an electromicrobalance and can be made of a variety of materials, as long as the plate becomes completely wetted; most common of which are filter paper, platinum, glass or mica.[73] The Wilhelmy plate is subject to two forces, the weight force F_p which acts

downward, and the Archimedes buoyancy force, F_a which acts upwards.[69] This can be expressed as shown in equation 3 where the total force on the Wilhelmy plate can be expressed as a function of the surface tension of the monolayer, γ_o, width of the plate and the forces acting upwards and downwards.

$$F = F_p + 2\gamma w - F_a \quad (3)$$

As the monolayer is compressed the lateral forces change while all other forces remain constant (F_p and F_a), because surface tension is defined as the change in surface pressure the tension can be expressed shown in equation 4:

$$\Pi = \frac{-\Delta F}{2w} \quad (4)$$

These equations are able to express the relationship between surface tension and surface pressure. They also indicate the importance of knowing the parameters of the Wilhelmy plate in order to control the monolayer compression.[73] Throughout this thesis project a Whatmann #1 filter paper was used as the Wilhelmy plate to measure the surface tension during the monolayer compression process.[73]

As mentioned in previous sections, as a Langmuir film is compressed there are typically four phases: a gaseous phase, liquid-expanded phase, liquid-condensed phase and solid phase. These phases occur in order as the monolayer is compressed. The gaseous

phase occurs immediately after the molecules are added to the interface, these molecules tend to spread across the surface of the interface with no exerted force in an effort to obtain thermodynamic equilibrium as mentioned above. As compression of the monolayer begins the molecules enter the liquid-expanded phase. Here the molecules are forced closer together and are subject to small amounts of attractive forces.[73] In the classic lipid example at this phase the hydrophobic tails experience some vertical alignment while remaining randomly ordered along the surface. As the compression continues the liquid-condensed phase is achieved resulting in a decreased area for the molecules to occupy and interactions between neighbouring lipids hydrophobic tails occurs.[73] Compressing the monolayer further still results in a solid phase, here the molecules are tightly packed and well ordered at the interface where all tails are oriented towards the air.[73] The solid phase is characterized by a dramatic increase in surface pressure and describes the linear relationship between the surface pressure and the molecular area.[64] Compressing a monolayer past this solid phase results in a collapse where molecules are forced from the surface of the liquid, causing the formation of unwanted multilayers. While the way in which nanorods behave at the air-water interface of the Langmuir-Blodgett trough is not completely understood, it is believed that the principles are the same and that the rods should behave similarly to lipids as the monolayer is compressed. It has been shown that the nanorods, specifically small aspect ratio rods orient themselves longitudinally along the interface so that at the right compression an ordered array with rods results, aligning end to end such that the monolayer produced is a 1D array.[75]

2.2 Electron Microscopy:

2.2.1 Scanning Electron Microscope:

Scanning electron microscopes were first introduced to the unenthused scientific community in the mid 1930's. At the time the development of the Transmission Electron Microscope (TEM) had already begun and the SEM was deemed an unnecessary tool.

Today SEM is recognized as a highly valuable instrument, which is able to provide information on crystal structure, electrical behaviour and composition among others. The SEM is a valuable tool in imaging due to its ability to preform non-destructive evaluations of samples.

The SEM has some primary advantages that are not present in other microscopes. The main advantages to the SEM includes the development of high brightness electron sources and field emission sources. The scanning electron microscope is advantageous due to its ability to provide 3D images of the samples which provides valuable information about the topography and morphology of the samples that are imaged. It also has advantages with regards to data acquisition. The SEM is fast and easy to use, provides high resolution images and requires minimal sample preparation, the data acquisition times are fast and a large depth of field is present.

The basic premise of the SEM is that a high energy, focused beam of electrons is scanned over a sample in such a way that an image of the sample is produced, primarily through the use of backscattered and secondary electrons. There are four main components in all scanning electron microscopes; the electron gun, anode, magnetic lens, and scanning coils. The electron gun is arguably the most important part of the SEM due to a key role it plays in the resolution of the instrument. The most common electron gun is the tungsten filament,

which have been in a majority of SEMs over the past 70 years due to their reliability and low cost.[76] With this type of gun the filament is formed into a V-shaped hairpin approximately 100 µm in diameter. As this filament is heated to temperatures greater than 2800 K, electrons are accelerated towards the anode component of the SEM. A tungsten filament is an inexpensive choice of electron source; however, it is unable to provide the resolution possible with a field emission electron gun.

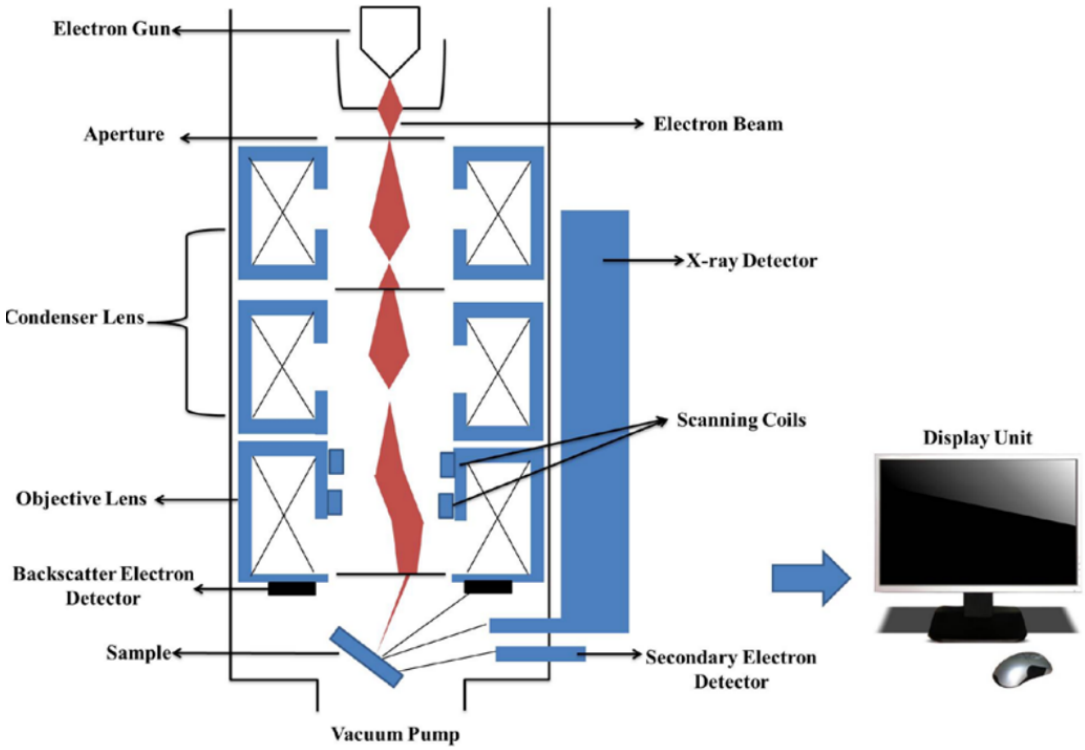

Figure 9: Schematic diagram of a typical SEM. Reproduced with permission from the author [73] Adapted from [82].

A field emission electron gun is a significantly more expensive electron source, the addition of this component increases the cost of the instrument substantially for a variety of reasons; including but not limited to an increased vacuum requirement. Field emission guns are typically made from a single tungsten crystal with an extremely sharp tip.[76] Rather

than heating the gun like a tungsten filament, the field emission guns produce electrons through the use of a strong electric field and the electrons are subsequently drawn towards the anode. Field emission guns come in three many varieties, Cold Field Emission (CFE), Thermal Field Emission (TFE) and Schottky Emitters (SE). CFE guns operate at room temperature; as a result, the emission of electrons relies solely on the electric field which is applied between the anode and cathode.[76] Thermal field emission guns, as is suggested by the name rely on the use of heat.[76] At elevated temperatures the adsorption of gases on the electron gun is reduced and the electron beam is stabilized.[76] Finally, there is the Schottky Emitter. This is very similar to the CFE both of which are preferred over the TFE guns. The Schottky emitter benefits from having the highest stability of the three types of field emission guns as well, due to the ease at which it can be operated.[76]

Field emission guns, such as the CFE are able to provide an 100x increase in electron brightness when compared to the standard tungsten filament as well as providing an increase in resolution down to 2 nm. However, as touched on briefly above, field emission guns require an ultra high vacuum system to stabilize electron emission and to prevent contamination. The vacuum system in an electron microscope is an extremely important, yet commonly overlooked component of the instrument. Electron beams are easily deflected and as a result to avoid this the electron microscope chamber needs to be free of any particles that could disrupt the beams pathway. To achieve the necessary chamber pressure of 10^{-9} – 10^{-10} Torr a combination of vacuum types is generally employed.[76] Most commonly a combination of mechanical, motor pumps are used to reach a pressure of 5×10^{-5} Torr at which point an ion pump, diffusion pump or turbo pump are

used to reach the necessary final pressure. In the most advanced system the chamber is void of everything except hydrogen atoms.[76]

In an SEM the anode has a positive bias which is used to attract the electrons emitted from the source. This positive bias serves to accelerate the electrons towards the next major component, the magnetic lens. The magnetic lens also known as the condenser lens plays an important role in focusing the electron beam. In most SEM chambers there exists two sets of condenser lens serving to produce a fine electron beam capable of passing through the aperture located within the column.[69,78-83] Several apertures present in the column ensure that the electron beam reaches the objective lens; which play a major role in focusing the electron beam on the sample and help determine the final diameter of the of the beam.[83]

The scanning coil, an additional component of the SEM serves the critical role of controlling the location of the beam. The scanning coil ensures that the electron beam always passes through the optic axis of the objective lens.[79-81] The electron beam is capable of penetrating up to 1.0 μm into the sample. All samples viewed using a SEM must be conductive otherwise an ultrathin layer of metal can be used to coat a non-conductive sample.[83]

The electron beam interacts with the samples in a variety of ways, all of which lead to the production of a different signal which can be analyzed with electron detectors.[78,80,82] The most common electron detectors are the backscattered electron detector and the secondary electron detector.[80-83] The secondary electron detector is used to detect the small numbers of electrons that are of a low energy (between 3 and 5 eV on average) and are contained near the surface of the sample. These electrons are emitted due to the surface

ionization that occurs when the primary electron beam interacts with the sample. Their low energy causes them to only be emitted a few nanometers from the surface of the sample, resulting in an image of the topography of the sample. The images most commonly associated with the SEM are a result of the secondary electrons and their interaction with the detector, where shadows occur when the part of the specimen is further from the detector.

The second most common detector contained within an SEM is the backscattered electron detector. This is used for the detection of high energy electrons and is defined as having an energy greater than 50 eV. As a result, the back scattered electrons usually arise from deeper within the sample. Backscattered electrons do not provide the same level of sample resolution as is associated with secondary electrons. However, they are used to provide valuable information regarding the sample's composition. Specifically, it is able to provide information about density differences within the sample. It should be noted that images obtained with the backscattered electron detector are brighter in areas that contain an element with a higher atomic number.

Additionally, in cases where elemental compositional information is desired the SEM can be equipped with an energy dispersive X-ray spectrophotometer (EDS) which detects the primary electron beam scatter as X-ray radiation.

The SEM is a valuable tool with applications in almost all scientific fields including but not limited to chemistry, geology, biology, medical science, and material science.[73] SEM has been used extensively in chemistry and material science for the analysis and characterization of nanoparticles.[73]

2.3 Ultraviolet – Visible Spectroscopy:

Ultraviolet – Visible spectroscopy is a technique which is used to quantify absorbed and scattered light.[84] In its most basic form a sample is placed between the light source and detector. The intensity of the beam before and after passing through the sample is measured, and the change in measured intensity is used to create a wavelength dependent extinction spectrum.[84]

Nanomaterials, particularly those made from gold and silver interact strongly with specific wavelengths of light. They exhibit optical properties that are sensitive to the size, shape, concentration and refractive index near the particle surface.[84] Studying the spectra obtained using this method, information regarding the optical properties of the nanomaterials can be obtained. Coupled with other characterization techniques such as scanning electron microscopy a correlation between shape and size of the nanomaterials to their optical properties can readily be made.

Chapter 3: Experimental Methodology

3.1 Reagents:

All glassware was immersed in an acid bath of 95-98% ACS grade sulfuric acid for a minimum of one hour unless otherwise stated, before being thoroughly rinsed with ultra-pure (Millipore) water (>18.2 MΩ cm) obtained from a Milli-Q plus system. This Millipore water was used to prepare all solutions unless specified otherwise. Glassware in which gold nanoparticle solutions were contained were washed with Aqua Regia (3:1 HCl and Nitric Acid), prepared fresh and rinsed thoroughly with Millipore water. All glass slides used for the preparation of the LSPR chip were first cleaned in Piranha Acid (3:1 Sulfuric acid: Hydrogen Peroxide) before functionalization. 3-APTMS purchased from Sigma Aldrich was used for silanation of the glass slides. Reagents used for the synthesis of gold nanorods were obtained as follows: Cetyltrimethylammonium bromide (CTAB) was purchased from BDH Chemicals, L- ascorbic acid and Silver nitrate (99.9999 %) from Sigma Aldrich, sodium citrate from ACP chemicals and mPEG-Thiol was purchased from Laysan Bio.

3.2 Synthesis of Silver Nanomaterials:

3.2.1 Silver Nanorods: standard procedure:

The seed mediated synthesis of silver nanorods was attempted using the standard Jana and Murphy method[85]. Briefly a seed solution was prepared by creating a 20 mL solution with a final concentration of 0.25 mM $AgNO_3$ and 0.25 mM trisodium citrate dihydrate in water. Under vigorous stirring, 0.6 mL of freshly made cold 10 mM $NaBH_4$ was added all at once. This seed solution was added to the growth solution after being left undisturbed for 2 hours.

The nanorod growth solution was prepared as follows; five sets of solutions were prepared each of which contained 0.25 mL of 10 mM $AgNO_3$, 0.50 mL of 100 mM ascorbic acid and 10 mL of 80 mM Cetyltrimethylammonium bromide (CTAB). To each of the solutions a varied amount of seed solution was added (2 mL, 1 mL, 0.5 mL, 0.25 mL and 0.06 mL). 0.10 mL of 1M NaOH was added to the mixture of seed and growth solutions, and then gently shaken. All solutions were prepared in vials and covered in tinfoil to minimize the amount of light allowed to react with the silver. However, no color change indicative of nanorod formation was observed.

3.2.2 Silver Nanorods Increased Concentration:

Variations to the Jana and Murphy method[85] for silver nanorod synthesis were attempted due to unpromising initial results. The amount of NaOH added was doubled and the concentrations of the $AgNO_3$ and the trisodium citrate were increased tenfold to 2.5 mM for the production of the seed solution. The use of a more concentrated seed solution yielded solutions in which the color changed from pale yellow to orange yellow and in some cases to a reddish colored solution. However, it was found that none of these color changes was indicative of nanorod formation.

3.3 Synthesis of Gold Nanomaterials:

3.3.1 Gold Nanorods – CTAB mediated growth:

The CTAB only synthesis for gold nanorods was adapted from the procedure outlined by Jiang et al.[86] A typical synthesis procedure is outlined in the next two sections. Resultant nanorods from this procedure were centrifuged at 5000 rpm for 30 minutes before being washed twice with 1.3 mL of Millipore water.

3.3.1.1 Seed Solution:

A typical seed solution had a resultant final volume of 8.65 mL, which contained 1.25 mL of 2 mM aqueous $HAuCl_4$ added to 2.74 mL of Millipore water in a 20 mL scintillation vial. To this solution, an additional 3.76 mL of 0.20 M CTAB solution was added and the contents were mixed. Finally, to the mixed solution, 0.9 mL of 10 mM ice cold $NaBH_4$ was added all at once, followed by vigorously shaking the solution by hand for 20-30 seconds. The resultant mixture was left to stand for 2 hours prior to use.[86]

3.3.1.2 Growth Solution:

In a similar fashion to the seed solution, the growth solution for the CTAB only nanorods was also adapted from the procedure outlined by Jiang et al.[86] The growth solution using this procedure had a resultant total volume of 8 mL comprised of the following; 1.6 mL of 2 mM $HAuCl_4$, 2.52 mL Millipore water, 3.8 mL of 0.20 M CTAB, 32 μL of 15 mM $AgNO_3$ and 51.2 μL of 0.1M of L-ascorbic acid, all added successively to a scintillation vial. After a brief mixing 34.7 μL of the seed solution was added. The solution was stirred vigorously for 20-30 seconds before being left to grow overnight.

3.3.2 Gold Nanorods – Binary Surfactant Synthesis:

3.3.2.1 Seed Solution:

Two different seed solutions were attempted in the standard growth solution outlined in the next section. Seed solution #1 is based on the method developed by the Murray group,[87] while seed solution #2 was developed by Khlebtsov et al.[88] While some of the steps in this procedure were experimented with (such as stirring and changes in concentration), the standard procedures for the seed solutions are outlined as follows.

Synthesis of Gold Seed Solution #1: The seed solution was prepared by mixing the following: 5 mL of 0.5 mM $HAuCl_4$, and 5 mL of 0.2 M CTAB in a 20 mL scintillation vial. Then 0.6 mL of a fresh ice cold 0.01 M $NaBH_4$ solution was diluted to 1 mL and added to the vial containing the $HAuCl_4$ – CTAB mixture being stirred at 1200 rpm. After two minutes the stirring was stopped. The solution color changed from yellow at the time of the addition of the $NaBH_4$ to a brownish yellow at the completion of the stirring. The seed solution was aged for two hours before being added to the growth solution.

Seed solution #2: This seed solution was prepared by adding 0.025 mL of 10 mM $HAuCl_4$ to 1 mL of aqueous 0.1 M CTAB in a scintillation vial mixed by swirling the solution. To this solution 1 mL of 10 mM fresh ice cold $NaBH_4$ was added and was stirred for 30 seconds over which time the color changed from brown to red. This was left for 2 hours before it was added to the nanorod growth solution prepared containing oleic acid.

Seed solution #1 by the Murray group was determined to produce the best rods for this project.[85]

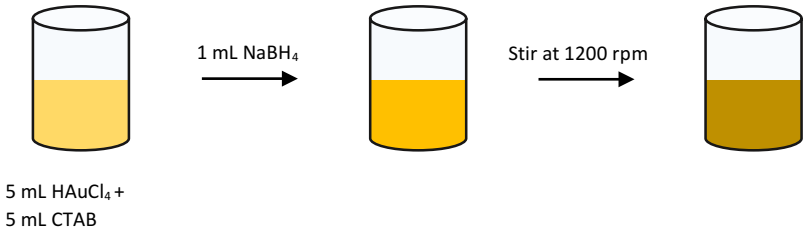

Figure 10: Schematic diagram for the production of seed solution #1

3.3.2.2 CTAB and Oleic Acid Growth Solution Synthesis:

The growth solution for the gold nanorods was prepared using the corresponding concentrations for a solution containing 7.0 g of CTAB, the synthesis was done at one tenth the scale. To begin, 0.70 g of CTAB and 0.1279 mL of oleic acid were dissolved in 25 mL

of warm water (~ 50 °C) in a 100 mL beaker. The solution was allowed to cool to ~ 30°C and then 1.8 mL of 4 mM $AgNO_3$ was added. This mixture was left undisturbed for 15 minutes at which time 25.0 mL of 1 mM $HAuCl_4$ was added. The solution was then stirred for 90 minutes at 700 rpm before 0.210 mL of 12.1 M HCl was added to the solution in order to adjust the pH to approximately 1.35. The solution was then permitted to stir for another 15 minutes at a slower stirring rate of 400 rpm prior to the addition of 0.125 mL of 0.064 M ascorbic acid. The solution was then stirred vigorously for an additional 30 seconds. To this solution 0.02 mL of the seed solution was added, stirred for another 30 seconds, and then left undisturbed at room temperature overnight (~ 12 hours) to allow growth.

3.3.2.3 CTAB and Sodium Oleate Growth Solution Synthesis:

The growth solution for the gold nanorods was prepared using the appropriate concentrations for a solution containing 7.0 g of CTAB once again at one tenth scale. To start, 0.70 g of CTAB and 0.1234 g of sodium oleate (NaOL) was dissolved in 25 mL of warm water (~ 50 °C) in a 100 mL beaker. The solution was allowed to cool to ~ 30°C and 1.8 mL of 4 mM $AgNO_3$ was added. This mixture was left undisturbed for 15 minutes after which time 25.0 mL of 1 mM $HAuCl_4$ was added. The solution was then stirred for 90 minutes at 700 rpm before 0.210 mL of 12.1 M HCl was added to the solution to adjust the pH. The solution was allowed to stir for another 15 minutes at a slower stirring rate of 400 rpm prior to the addition of 0.125 mL of 0.064 M ascorbic acid. It was then stirred vigorously for an additional 30 seconds. To this solution 0.02 mL of the seed solution was added, stirred for another 30 seconds, and it was then left undisturbed at room temperature over night (~ 12 hours) to allow growth.

For nanorods prepared using this growth solution, the seed solution follows protocol #1 except for the amount of time that the seed was allowed to age. In this case the seed solution was aged for only 30-40 minutes.

3.3.3 Isolation of Nanomaterial Colloid:

Nanorods are isolated from the bulk solution using centrifugation. The bulk solution is added to centrifuge tubes in 1 mL increments and centrifuged at 7000 rpm for 30 minutes. The supernatant is then removed and 1 mL of ultrapure water is added to the obtained colloid to wash away residual CTAB before it is centrifuged a second time at 7000 rpm for 30 minutes. The supernatant is removed and the colloidal solution is then collected in a clean scintillation vial.

3.4 PEGylation of the Nanorods:

Using nanorods prepared via the binary surfactant method, CTAB was replaced with methoxy polyethylene(glycol) thiol (mPEG-SH or mPEG-thiol). This step is used to ensure that all possible interference caused by CTAB is minimized; at both the air water interface and in further sensing applications.

5 mL of the m-PEG-SH (MW 5000) solution was prepared using 0.1200 g of m-PEG-SH. To 12 mL of the obtained nanorod colloid described previously, 13 μL of mPEG-SH was added. The resultant solution was stirred overnight to ensure even coating of the nanorods. The mPEG-SH solution was stored in the fridge to preserve shelf life.

3.5 Formation of Nanorod Monolayers:

Nanorod monolayers were prepared using the Langmuir-Blodgett system. The Teflon® trough and Delrin® hydrophilic barriers were cleaned with ethanol and rinsed

thoroughly with Millipore water. It was later found that this was not successfully removing the residual gold rods from the trough and the cleaning procedure was adapted to cleaning with chloroform and rinsing with water. The trough was then filled with Millipore water (approximately 750 mL), the Whatmann paper was hung from the balance and the temperature probe submerged in the water being sure to avoid contact with the bottom of the trough. The surface of the water was cleaned using a gentle vacuum suction to remove any noticeable dust. A certain volume of nanorods dispersed in chloroform were deposited carefully dropwise onto the surface of the water using a Hamilton syringe. After 15 – 30 minutes (allotted time to allow the chloroform to evaporate) the nanorods were compressed at the air-water interface at a certain rate until the desired surface pressure was reached. The surface pressure value was varied in attempts to form the best monolayer. The monolayer was transferred to a silicon wafer, which was attached to a carbon screen printed electrode. This was done at a temperature of 20 - 30 °C and controlled using a circulating water bath. The Millipore water was used so that high resolution SEM images could be obtained. Transfers were attempted at high and low humidity to determine optimal conditions. The monolayer was added to the silicon chip using the Langmuir – Blodgett method. The chip was left to dry at room temperature overnight before being imaged by SEM.

3.5 Instrumentation:

All the instrumentation used in this thesis has its own standard operating procedure (SOP) which will be highlighted in the following sections.

3.5.1 Ultraviolet -Visible Spectroscopy:

Ultraviolet-Visible spectroscopy is one of the primary tools used for this work and was used in two main ways: to measure the longitudinal and transverse peaks associated with the synthesized nanorods, and for monitoring the wavelength shift for the produced LSPR substrate; wavelength shifts in the longitudinal peak are monitored for the LSPR sensor.

3.5.1.1 Bulk nanorod Sample:

The Cary Bio 50 UV-Vis Spectrophotometer was used to measure the longitudinal and transverse peaks associated with the gold nanorods. Measurements were taken only after setting the baseline correction to correct for water, to remove any unnecessary background. The samples were then prepared by taking an aliquot of the bulk nanorod growth solution and adding it to a standard quartz cuvette until it was approximately one-third full, prior to filling the rest of the cuvette with Millipore water. Samples were scanned using the fast setting from 200 – 1000 nm. If the whole spectrum could not be viewed between 200 and 1000 nm the scanning parameters were extended to 1100 nm. Measurements were saved in a file format compatible with Origin, and data analysis was completed in Origin 8.

3.5.1.2 LSPR Chip Based Sample:

For LSPR based measurement the Cary Bio 50 UV-Vis spectrophotometer could not be used for the solid substrate. As a result, the Ocean Optic 2000+ spectrophotometer was used instead in absorbance and transmission mode.

The LSPR chips in this case were prepared by sonicating the previously piranha acid cleaned glass coverslips, in a 5:1:1 v/v % Millipore water / hydrogen peroxide / ammonium hydroxide solution. These coverslips were sonicated for 1 hour before being

rinsed well with Millipore water. Finally, the substrates were incubated in a 1 % v/v solution of 3-Aminopropyltrimethoxysilane (APTMS) for a minimum of 2 hours. Prior to nanorod addition the prepared glass slides were rinsed with methanol and Millipore water.

Nanorods were added to the functionalized slides using two different methods. The first being a drop coat of rods onto the chip followed by air drying. The other being an incubation of the slide in colloidal nanorods for 24 hours.

3.5.2 Scanning Electron Microscope:

The Scanning Electron Microscope (SEM) was used to image all samples. Images were acquired using the Tescan MIRA3 LMU Field Emission SEM (Warrendale, PA, USA). This instrument is equipped with a high brightness Schottky emitter for high-resolution/high current/ low noise-imaging and a secondary electron detector. Images were acquired use an ultra-high vacuum mode at 20 kV. The SEM also contains an INCA X-max 80 mm 2 EDS system which can be used to detect elements present within a specified region of the SEM. This can be used to provide qualitative and semi-quantitative information. The detector used for this thesis work was a silicon drift detector (SDD).

SEM analysis was done to confirm the shape and size of the nanomaterials after the growth was complete. Between 3 – 5 μL of the colloidal nanoparticles were deposited onto a 5 x 5 mm silicon wafer, (Ted Pella, Inc., Redding, CA, U.S.A) and left to dry at room temperature. Langmuir - Blodgett transfers were completed on the silicon wafer as well, for the development of a uniform monolayer to make imaging easiest due to the atomically flat silicon surface.

3.5.3 Langmuir – Blodgettry:

The formation of a monolayer of nanorods at the air-water interface was accomplished using a KSV NIMA Langmuir-Blodgett trough and the accompanying software (Biolin Scientific, Finland). This instrument has been placed on top of a 6.50 cm thick marble slab in an effort to reduce vibrations and thus improve the film quality. The surface pressure measurements were acquired by hanging a 10 mm wide (20.6 mm perimeter) Whatman #1 filter paper from the microbalance. Subphase temperatures were controlled using a Lauda K-2/R circulating water bath (Brinkmann Instruments, NJ, USA) connected to the trough. The temperature of the subphase was monitored using a temperature probe which was submerged in the water (subphase) during the course of the

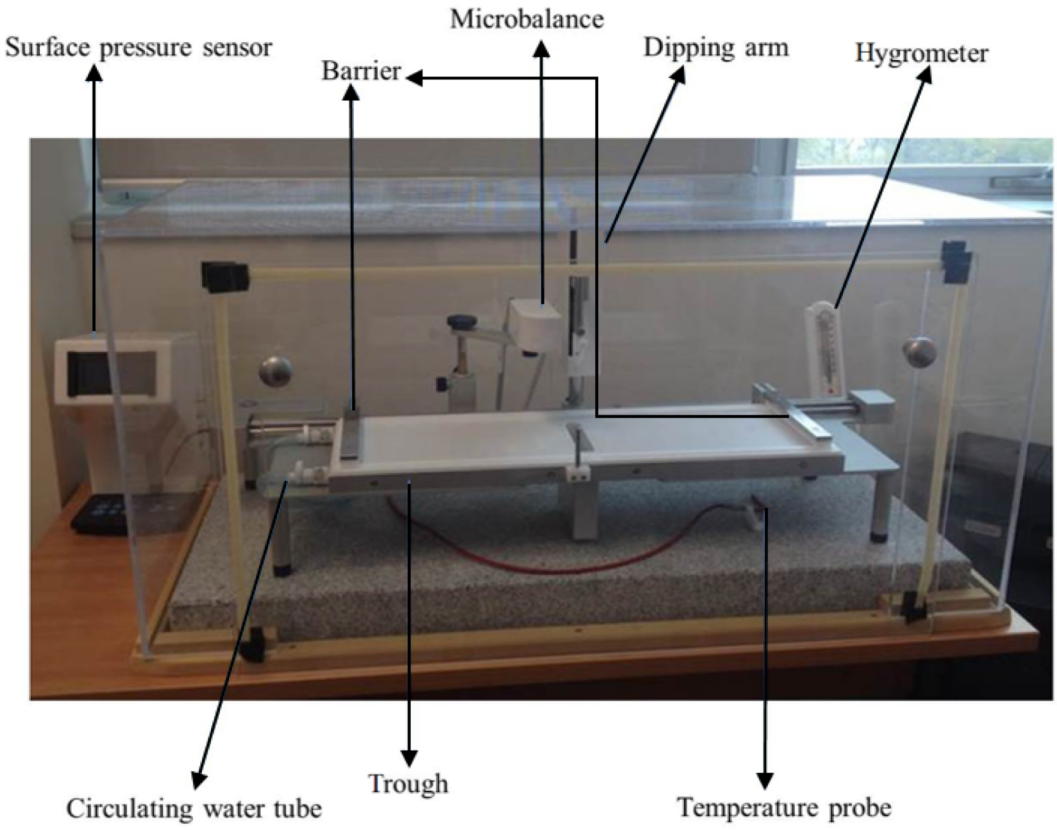

Figure 11: Langmuir Blodgett Schematic Diagram Adapted from reference [73]

experiments. To maintain precise control over the transfer of the monolayer to a solid substrate an automatically controlled dipping arm was used. A schematic representation of the Langmuir Blodgett can be seen in Figure 11.

Chapter 4: Results and Discussion

4.1 Nanorod Synthesis

4.1.1 Silver Nanorods:

Silver nanorods were attempted following the Catherine Murphy method of synthesis which is a wet chemical synthesis method. In this method silver seeds of approximately 4 nm in diameter were produced via a reduction of $AgNO_3$ with $NaBH_4$ in the presence of trisodium citrate. This seed was added to a growth solution as described in section 2.2.1. The expected results were a variety of solutions containing nanorods of different aspect ratios, ranging in color from a deep yellow to blue/green as the ratios increased.

The results yielded did not behave as expected. The introduction of the seed solution, which was a pale yellow solution, to the growth solution resulted in solutions of

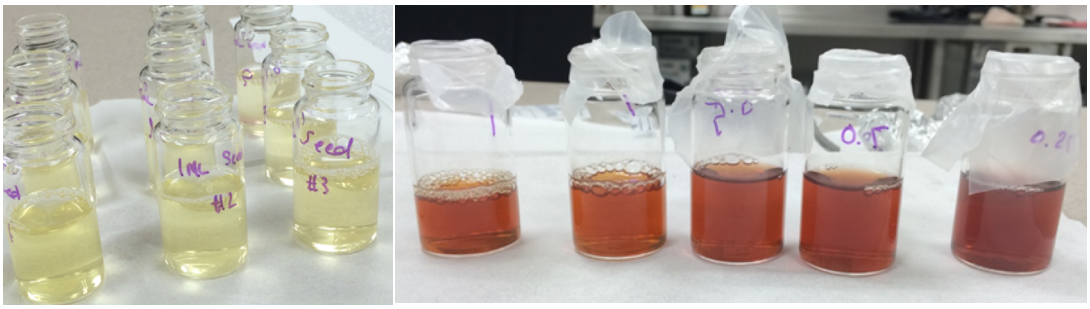

Figure 12: Attempts at growing silver nanorods.

either a varying degree of red or resulted in no color change at all. Figure 12 shows an example of variation in results yielded when attempting to synthesize the silver nanorods. None of the attempted syntheses resulted in the successful production of nanorods as would have been evidenced by two peaks in the UV-Vis spectrum. It is believed the synthesis of silver nanorods was unsuccessful due to a CTAB glassware contamination. These

assumptions however were not confirmed. Future experiments could be done to confirm this by using both UV-Vis, and the SEM with EDS attachment, analysing the sample for a high concentration of bromide ions. As a result of the difficulties producing silver nanorods, gold nanorod production was attempted instead.

4.1.2 Gold Nanorods - CTAB mediated Growth:

The first successful nanorod synthesis was yielded by attempting the CTAB mediated gold nanorod growth method. Using the procedure outlined in the experimental section 2.3.1 gold nanorods were produced. This method suffered from inconsistency and it was noted all experiments could be replicated precisely multiple times and still not successfully yield the same results. This can be seen in Figure 13, in which all vials contain the growth solution in the same amounts and the same amount of seed solution and yet the results are vastly different; both in colour and in the successful synthesis of the nanorods.

Differences in the UV-Vis spectra obtained for the gold nanorods produced using this procedure can been seen in Figure 14. This figure primarily shows the inconsistencies that resulted from using this procedure. While the formation of rods did occur in each flask, for this experiment to be considered a success it would have been necessary for all of the rods formed to contain the same relatively sharp λ_{max} peak indicating the formation of uniformly sized nanorods. The broadening of the peaks shown in Figure 14 indicates that the rods have not grown in a uniform manner.

It was noted that using this synthetic method that the amount of time the rods were allowed to grow greatly affected the results. Keeping the bulk solution of nanorods for more than a few days was therefore not beneficial. Figure 15 shows the obtained SEM images for these nanorods.

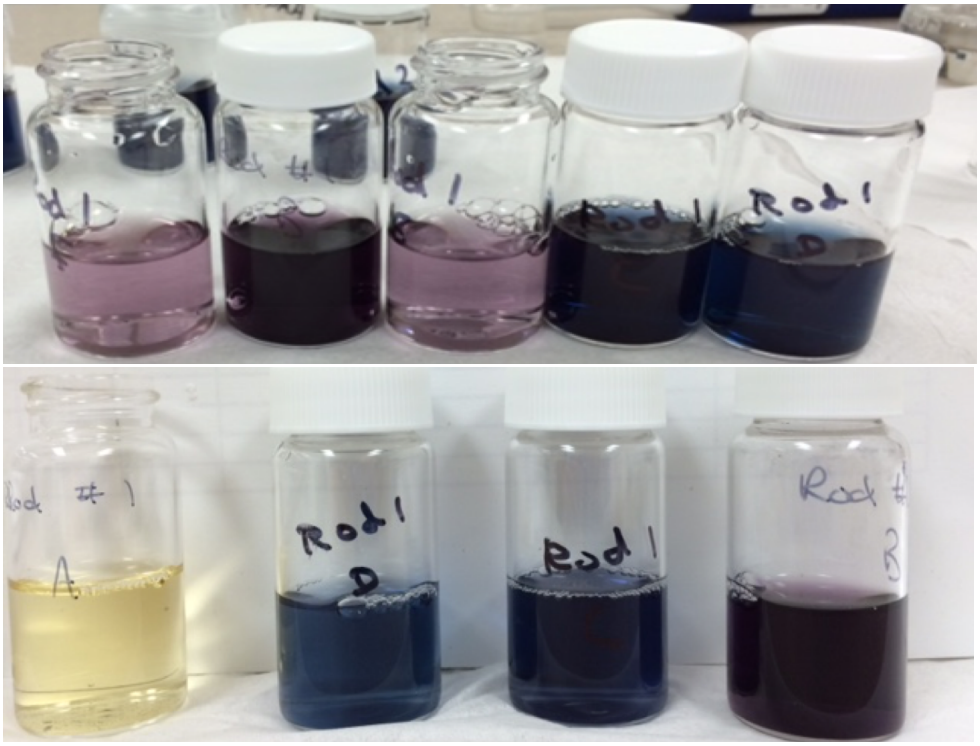

Figure 13: Gold Nanorod synthesis using CTAB only seed mediated growth method

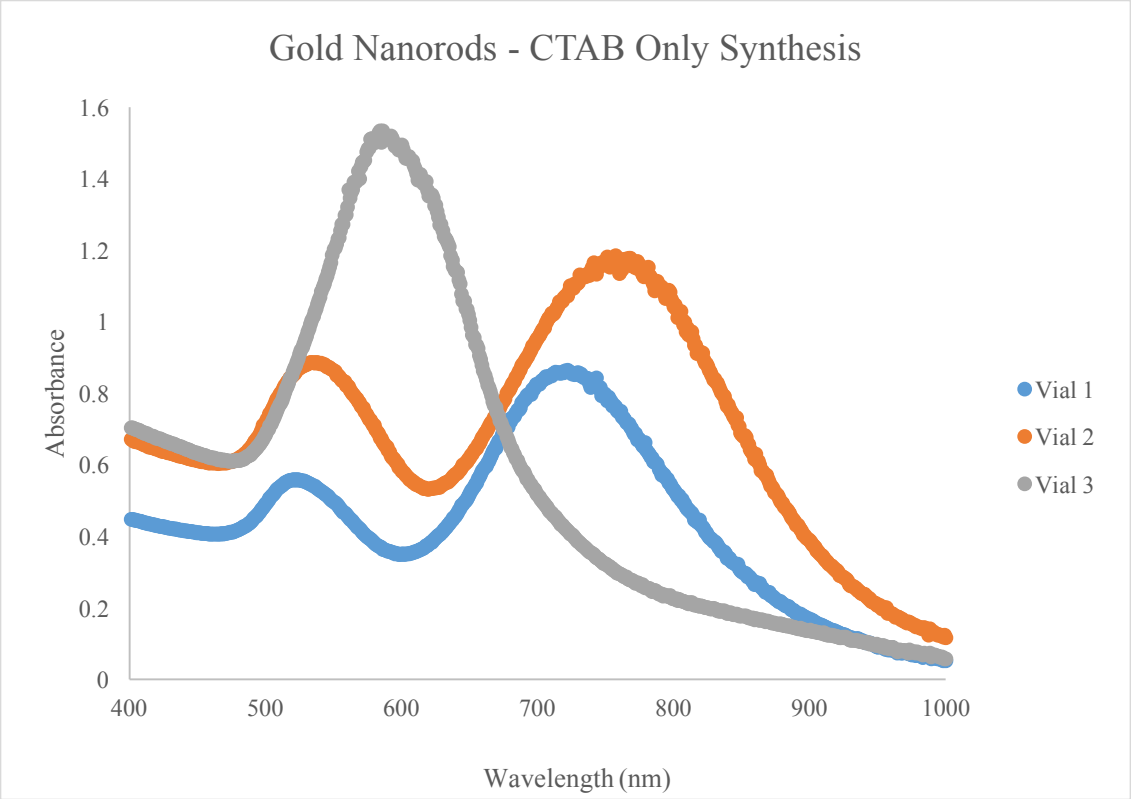

Figure 14: A subset of the different UV-Vis spectra obtained for the gold nanorod seed mediated growth containing only CTAB, where each color represents a different rod growth solution.

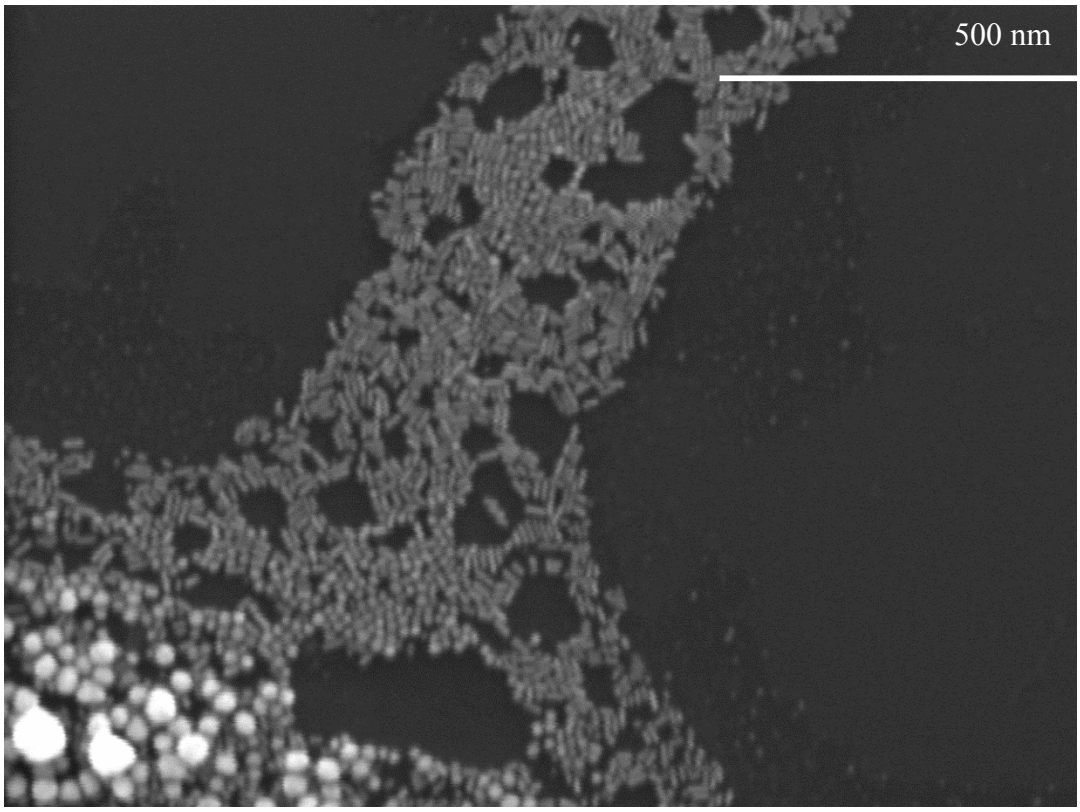

Figure 15: SEM images for gold nanorods CTAB only procedure

4.1.3 Gold Nanorods – Binary Surfactant Nanorod Growth – Oleic Acid

Using the binary surfactant growth method outlined in Section 2.3.2 gold nanorods were synthesized.[87] This growth procedure produced rods with a longitudinal λ_{max} value of 820 nm 2 hours after the addition of the seed and 776 nm after sitting undisturbed for 23 hours. Interestingly the results indicate a blue –shift in the λ_{max} values of the nanorods. However, the longitudinal peak exhibited also indicates a change in uniformity of the rods, indicated by a decrease in the degree of peak broadening shown in Figure 16. These nanorods were imaged using SEM and while nanorods were clearly present there was also a surplus of spheres. In the synthesis of nanorods it is widely accepted that spheres are indicators of impurities. In this case it is unclear if the spheres are simply nanorods which

are standing on end. Further imaging using transmission electron microscopy is needed for conclusive determination if the spheres are present.

This nanorod synthesis was repeated to ensure that the results were reproducible and the resultant rods had a λ_{max} value of 743 nm after 23 hours rather than the 776 nm observed after the first synthesis. It is understood that this peak maximum is related to the aspect ratio of the nanorods.

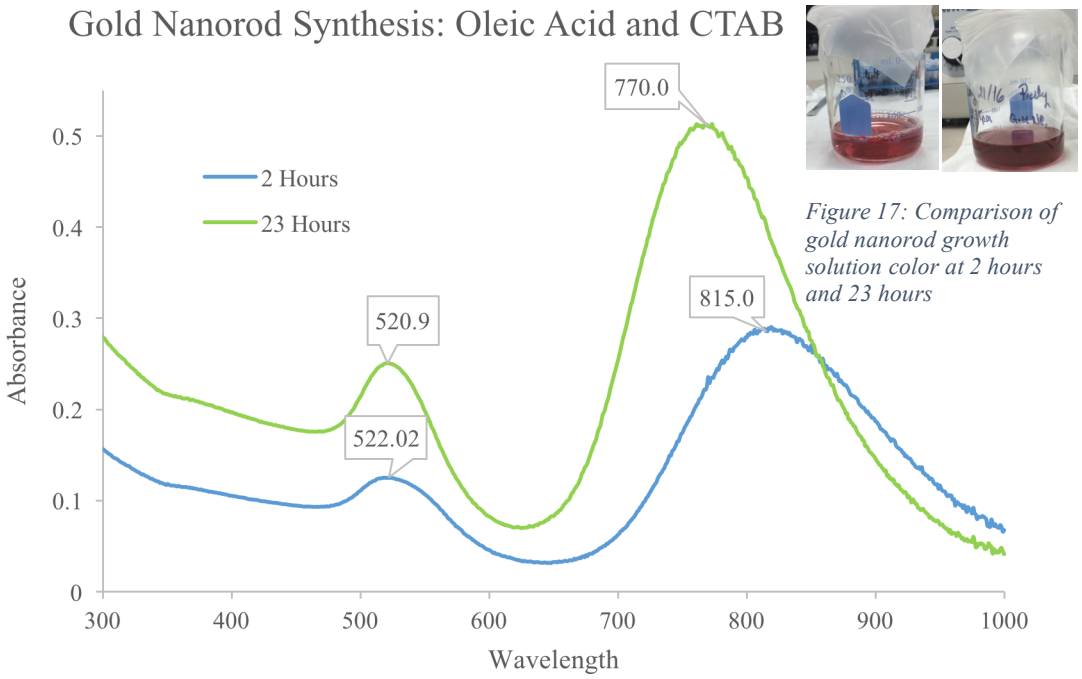

Figure 17: Comparison of gold nanorod growth solution color at 2 hours and 23 hours

Figure 16: UV-Vis spectra obtained for Oleic Acid Binary surfactant nanorod synthesis

While all results obtained with this method were promising, it was noted that the oleic acid did not mix as expected in the growth solution. Upon addition of the oleic acid to the growth solution some kind of precipitate formed which didn't completely dissolve. It was also noted by analyzing the SEM corresponding to this synthesis that while rods

were successfully formed, there was a high number of spheres present in the obtained colloid. However, due to the successful and repeatable rod formation with oleic acid it was determined that this procedure was promising for the formation of nanorods. As a result, moving forward all nanorods were made following this procedure but sodium oleate (NaOL) was used instead of oleic acid, as outlined in the literature.[87,88]

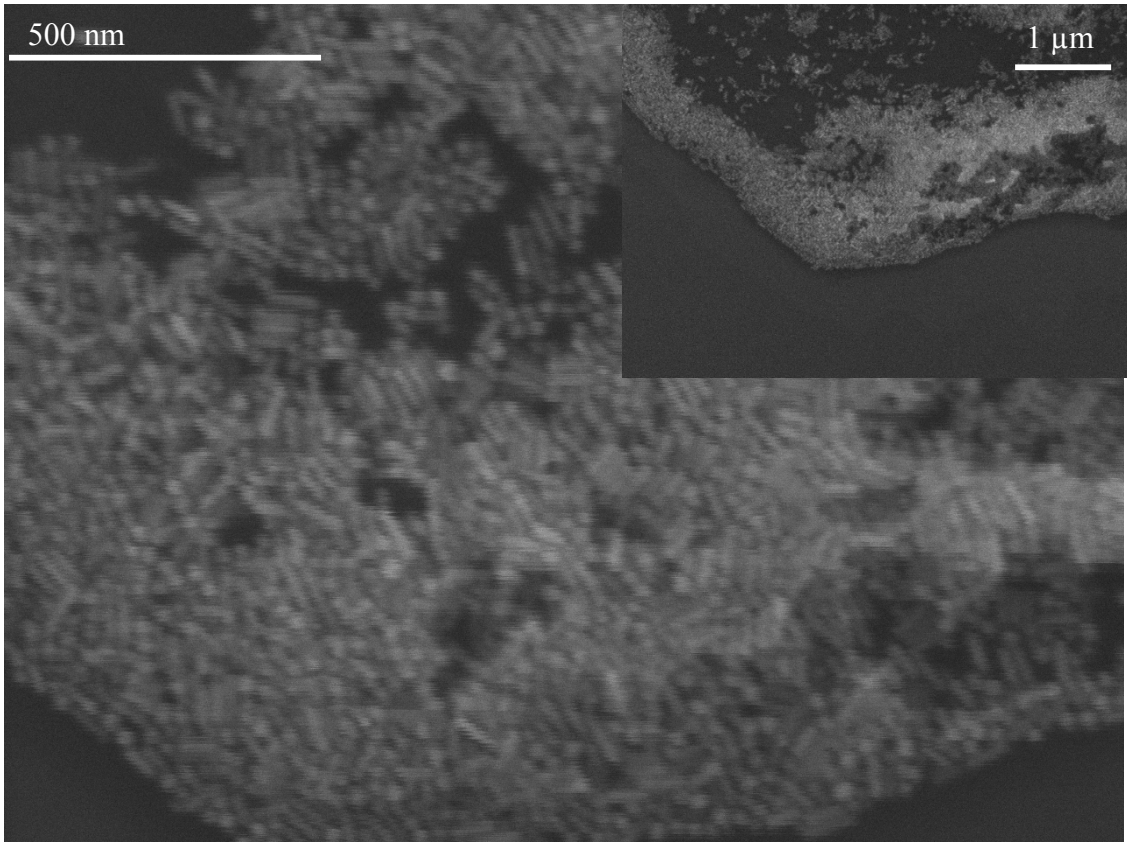

Figure 18: SEM images of gold nanorods synthesized using CTAB and Oleic Acid. SEM studs prepared using washed colloids. Overlay shows the sample at a distance of 1 µm away.

4.1.4 Gold Nanorods – Binary Surfactant Nanorod Growth – Sodium Oleate:

Success with the binary surfactant method for synthesizing gold nanorods using oleic acid lead to attempting the synthesis with sodium oleate (NaOL) as outlined in the

literature.[87,88] This synthesis is an exact replica of the previous synthesis with the only change being the use of NaOL instead of oleic acid. This change successfully resulted in the synthesis of nanorods while also eliminating some of the sphere impurities found while using oleic acid. This synthesis also produced rods with a λ_{max} value of approximately 790 nm; an ideal wavelength for this project.

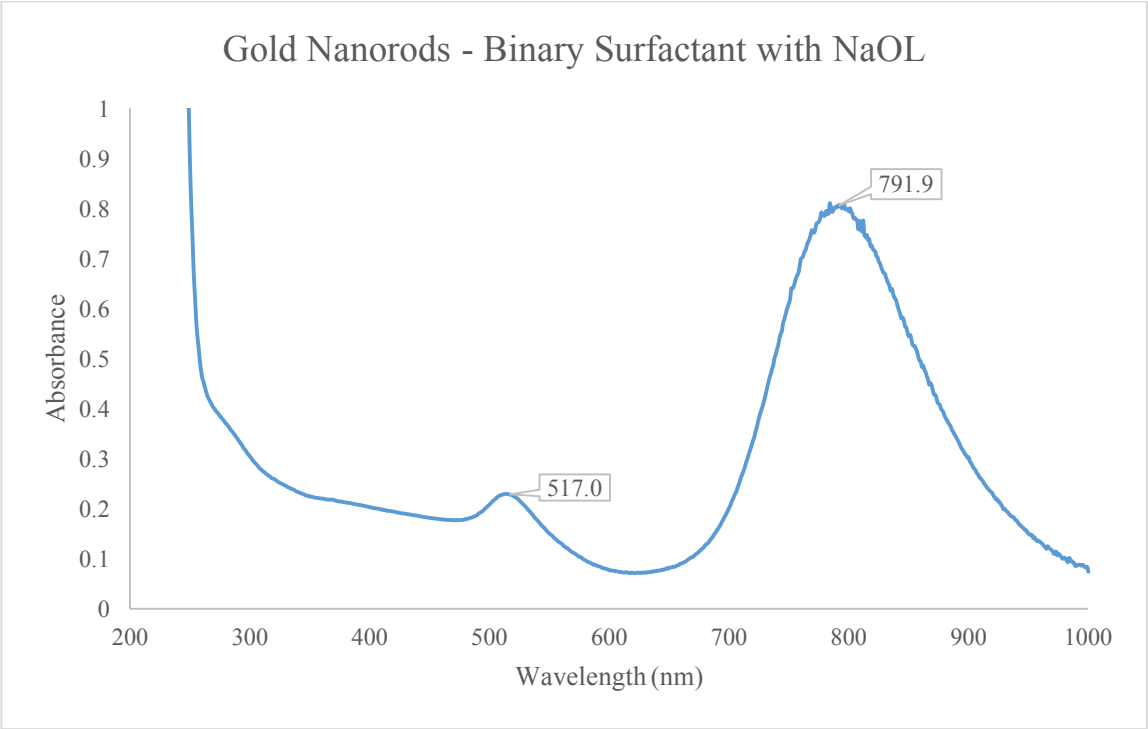

Figure 19: Binary surfactant method of gold nanorods synthesis using sodium oleate.

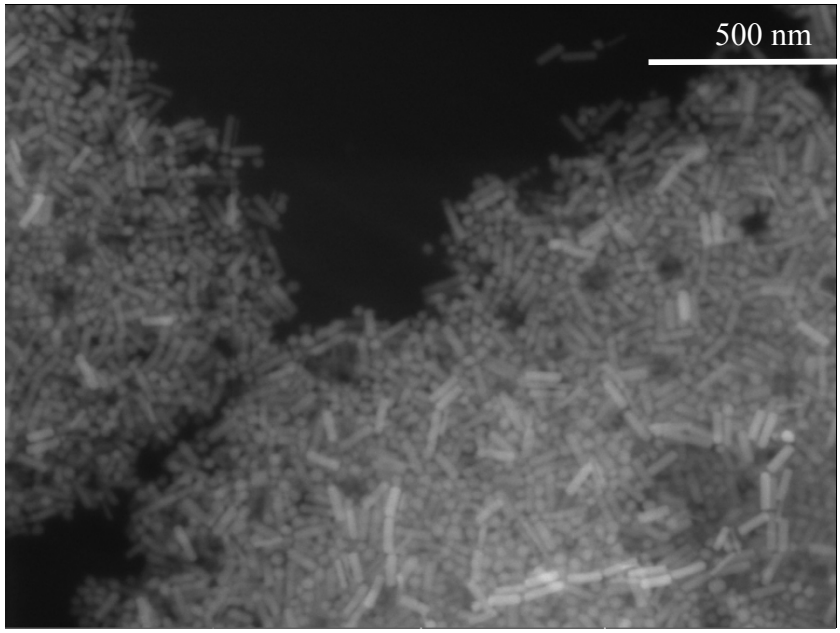

Figure 20: SEM image of gold nanorods produced using sodium oleate binary surfactant method.

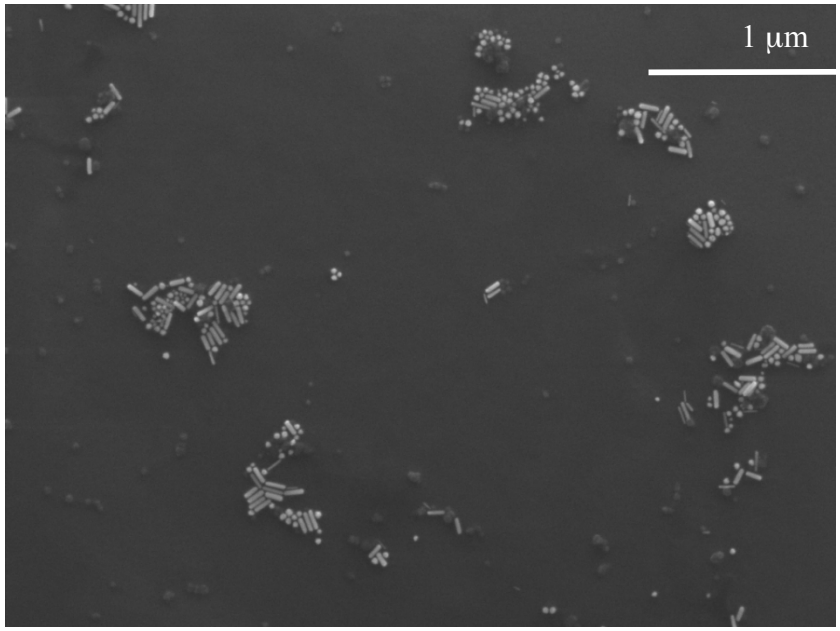

Figure 21: SEM image of gold nanorods produced using sodium oleate binary surfactant method.

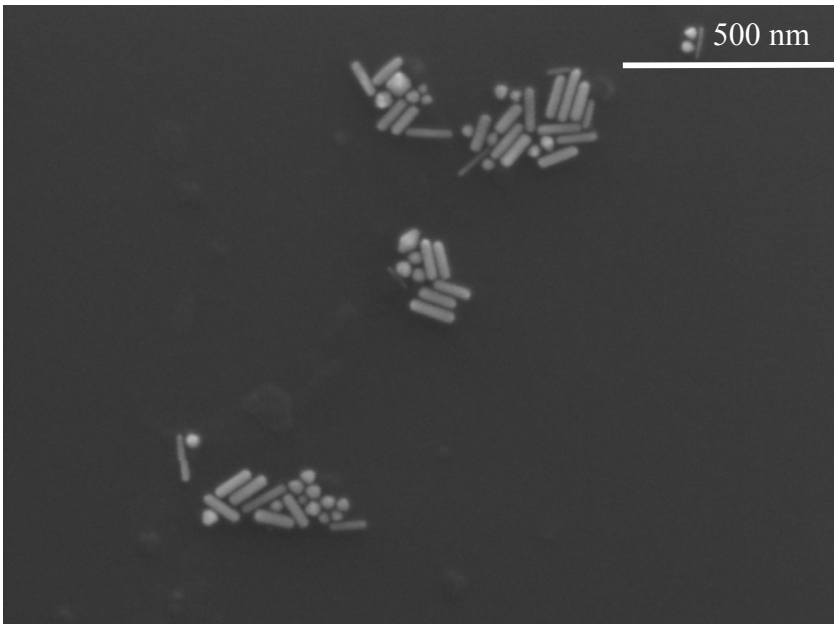

Figure 22: SEM image of gold nanorods produced using sodium oleate binary surfactant method

4.1.5 Nanorod Synthesis Summary:

In summary it was found that both the silver and gold nanorod synthetic methods containing only CTAB as a surfactant were unsuccessful, and/ or unreliably reproducible. This problem was overcome by using the binary surfactant method of nanorod formation.[87,88] Some variations of this method lead to the conclusion that the most reproducible nanorods were produced using sodium oleate, rather than oleic acid, as a well-mixed solution could be obtained which was not possible using oleic acid due to the precipitate.

Various parameters were tested in an attempt to optimize the aspect ratio of the rods including growth time and age of the seed solution. It was determined that for the production of long thin nanorods the seed solution must be no older than 30-45 minutes. For nanrods with a slightly smaller aspect ratio an older seed solution is ideally aged

approximately 2 hours, similar to what is done for the CTAB only nanorod syntheses.[89] Letting the seed solution age for 2 hours was found to produce rods with a λ_{mac} value of approximately 770 – 790 nm which is ideal for sensing applications.

While this synthesis was able to successfully produce nanorods, there are still some nanoparticle impurities in the bulk solution which can be seen in Figure 20 - Figure 22. Ideally all nanoparticles should grow into a nanorod, however, since this is not the case, steps to minimize impurities may be needed for future applications.

4.2 Functionalizing the Nanorods:

It was determined that the optimum nanorod synthesis was obtained using the binary surfactant method of synthesis.[87,88] From this point onward all nanorods are produced via this method. It was determined that the presence of CTAB would lead to issues with respect to using the nanorods for anticipated sensing applications. The presence of CTAB was expected to cause problems with Langmuir Blodgett applications as well. Removal of the CTAB was attempted to limit the potential interferences, and to functionalize the rods so that they were better suited for Langmuir-Blodgett applications.[90]

4.2.1: PEGylating the Nanorods:

It has been previously shown that CTAB can be replaced with a thiolated polyethylene glycol.[91-95] mPEG-SH was added to colloidal nanorods and the effect of the addition was monitored using SEM. This can be seen in Figure 23-Figure 25. Most noteworthy is the evidence of a coating or shell which can be seen surrounding the nanorods depicted in Figure 25. A comparison can be done with these nanorods to the rods prior to PEGylation which are depicted in Figure 22. Thiol groups are known to readily bond to gold nanomaterials.[96] Due to the evidence of the shell surrounding the nanorods it

can be determined that the sulfur in mPEG-SH has displaced at least some of the CTAB allowing for the mPEG-SH to remain coated on the nanorods.

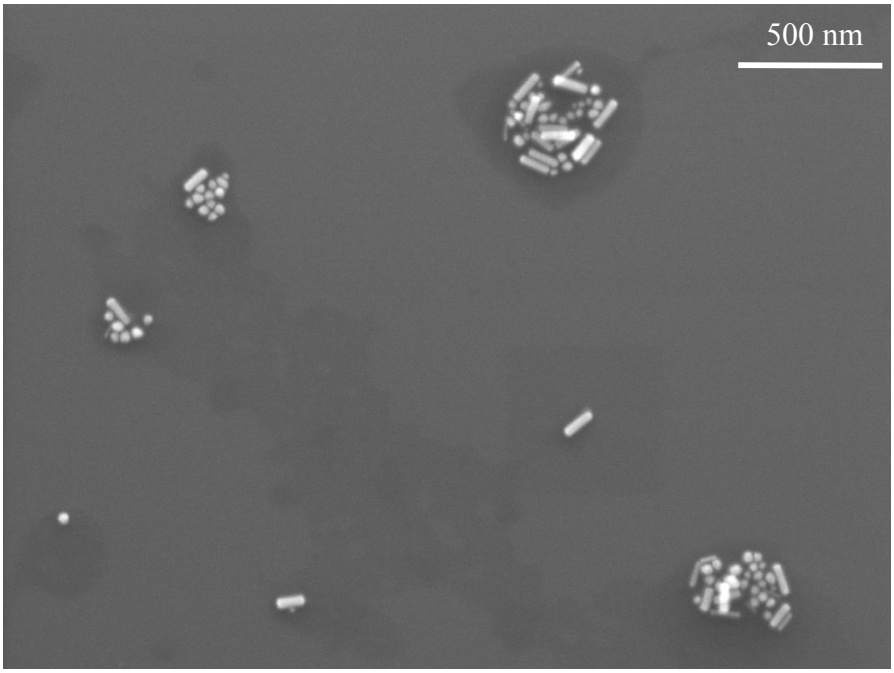

Figure 23: SEM image of mPEG-SH nanorods.

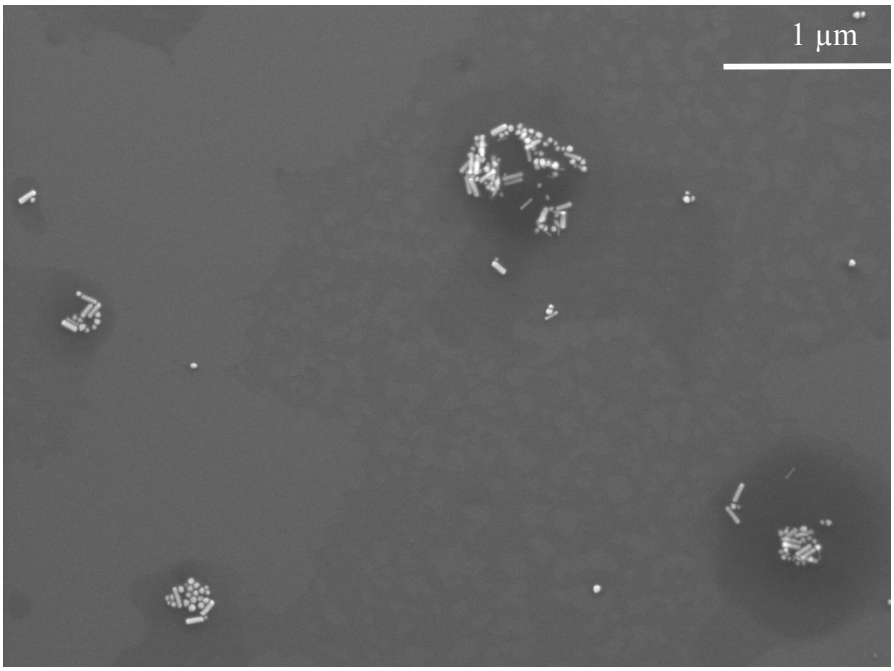

Figure 24: SEM image of mPEG-SH nanorods.

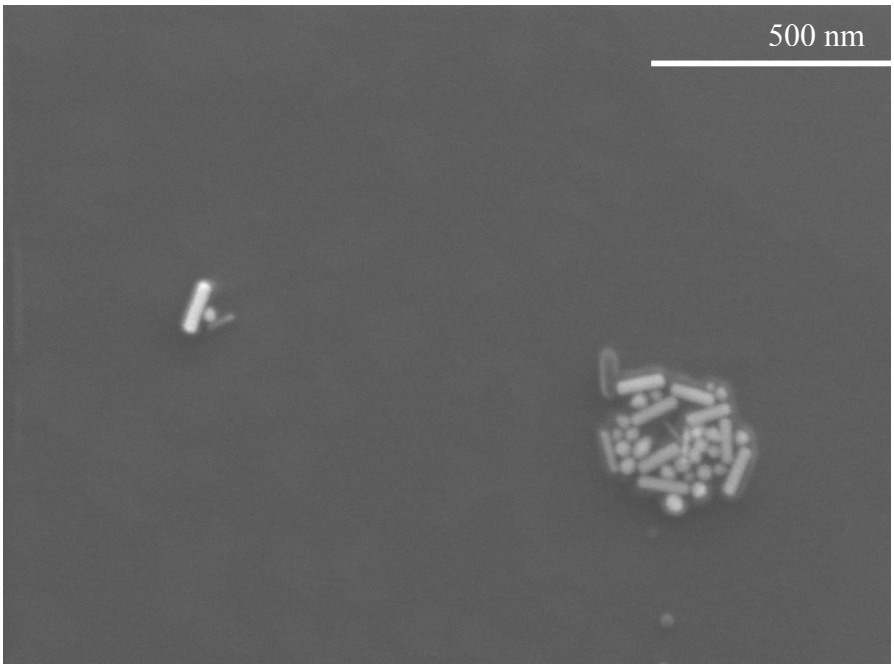

Figure 25: SEM image of mPEG-SH nanorods.

4.2.2 Functionalization Summary:

In summary because the mPEG-SH appeared to be an effective means of replacing the CTAB, this was the only method used to replace CTAB. Based on the knowledge that sulphur bonds readily to gold nanomaterials mPEG-SH coated rods should behave in a hydrophilic manner if added to the air-water interface of the Langmuir - Blodgett trough in future experiments. [96]

4.3 Langmuir Blodgett Monolayers:

In the standard monolayer formed using the Langmuir – Blodgett, lipids are spread at the air-water interface using a volatile organic solvent such as chloroform. In studies using nanorods instead of lipids, attempts were made to form monolayers by varying parameters associated with the Langmuir – Blodgett. The standard technique was varied so that the effect could be monitored. Some of these parameters include surface pressure, compression rate, presence of chloroform, effect of PEGylating the nanorods, etc.

4.3.1 PEGylated Nanorods

Colloidal nanorods which were functionalized with mPEG-SH were added to a thoroughly cleaned Langmuir-Blodgett trough. Dispersing the rods without chloroform was attempted many times yielding various results. During some of the first trials with the PEGylated rods, aggregates clearly formed in the syringe prior to the deposition. In this case the rods were not successfully transferred to the silicon chip in a monolayer. In an attempt to minimize aggregation, some experiments in which chloroform was added to the colloid were analyzed.

The addition of the PEGylated nanorods to the air–water interface yielded a variety of results. Figure 26 and Figure 27 show the results obtained by PEGylating the colloidal

nanorods and introducing them to the air-water interface without the use of a volatile solvent such as chloroform to enhance spread-ability at the air-water interface. In Figure 28 and Figure 29 the results of a Langmuir-Blodgett transfer of PEGylated nanorods dispersed in chloroform, which have first been centrifuged to remove excess PEG are shown. In these images it should be noted that the rods have aligned themselves with one another in small quantities. These nanorods have also effected what is known as the "coffee ring effect".[97,98] The formation of this effect on the substrate is believed to be caused by the speed at which the substrate has dried causing the rods to orient themselves in spherical shapes caused by water droplets drying. Finally in Figure 30 and Figure 31 the transfer of PEGylated nanorods in the presence of chloroform without the removal of excess PEG-SH has been analyzed. It was determined from these results that the best coverage of the substrate was obtained when the nanorods were dispersed in chloroform like that shown in Figure 28 and Figure 29.

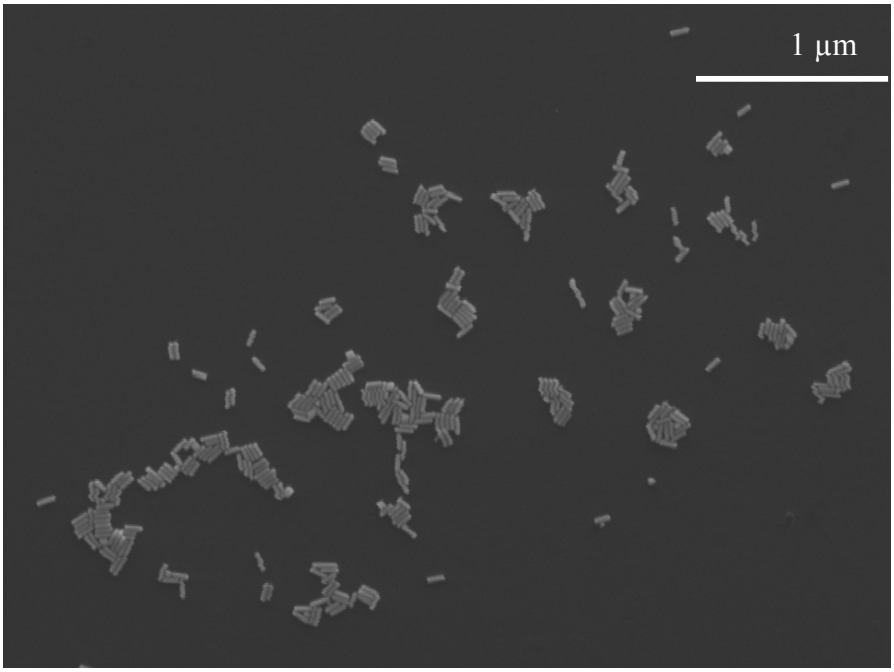

Figure 26: Colloidal PEGylated nanorods not dispersed in chloroform.

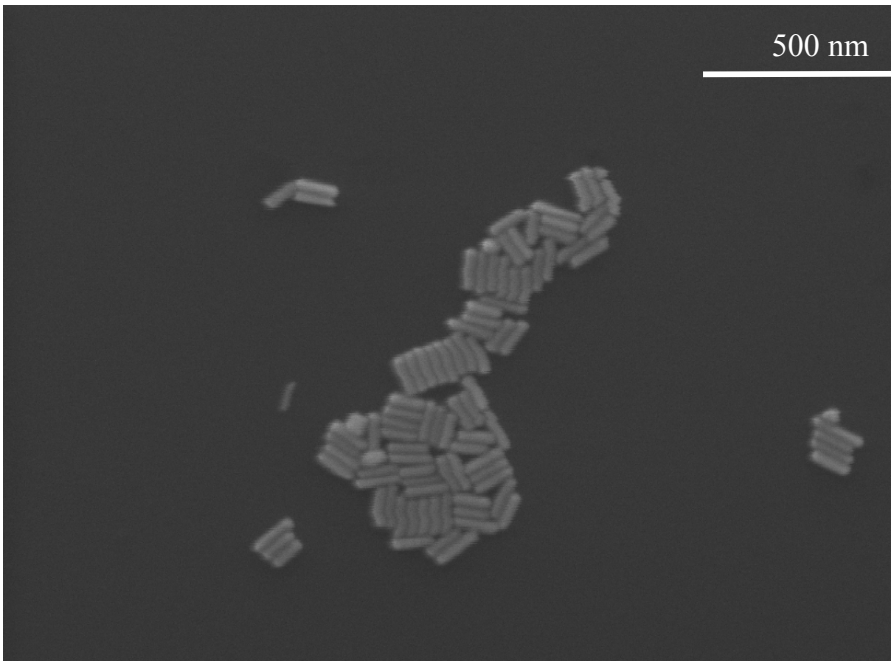

Figure 27: Colloidal PEGylated nanorods not dispersed in chloroform..

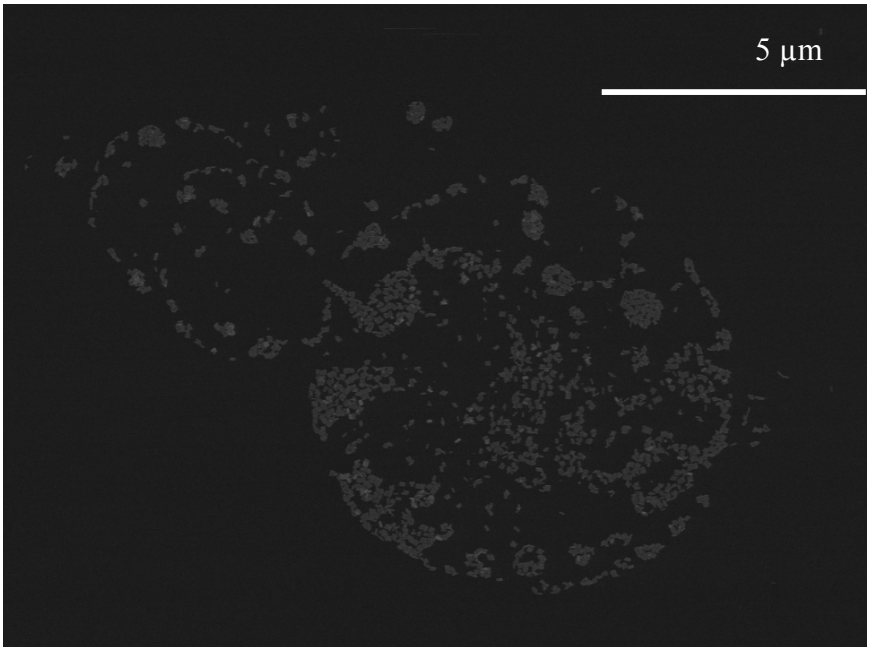

Figure 28: PEG-SH colloidal nanorods dispersed in chloroform added to the air-water interface

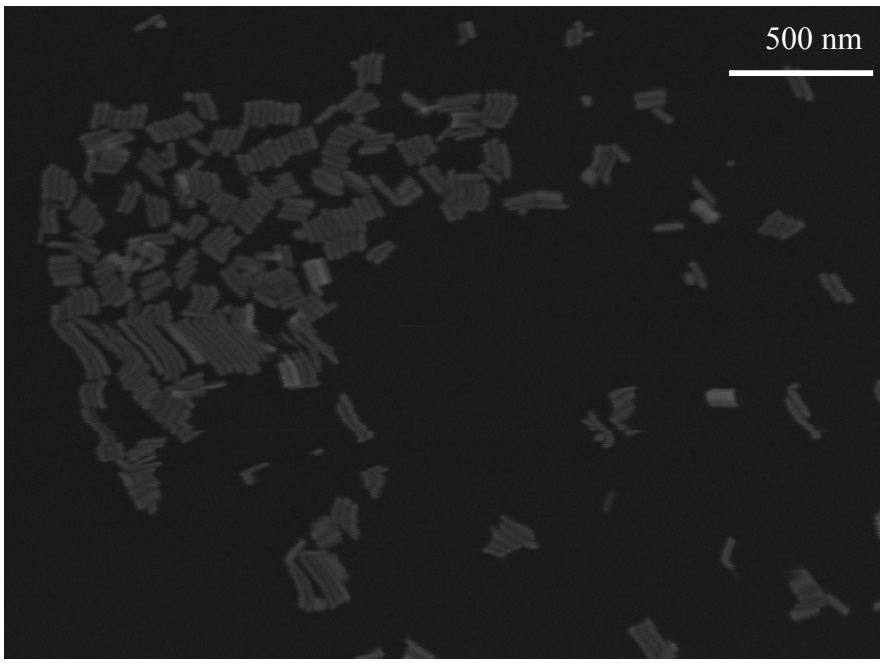

Figure 29: PEG-SH nanorods colloid, dispersed in chloroform added to the air-water interface.

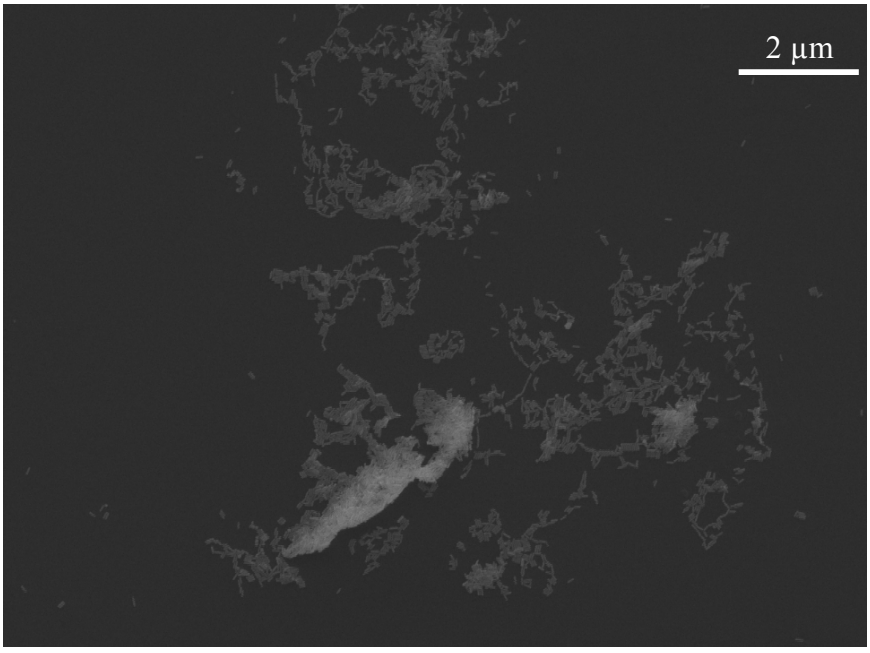

Figure 30: PEG-SH nanorods which have been dispersed in chloroform prior to the removal of excess PEG-SH.

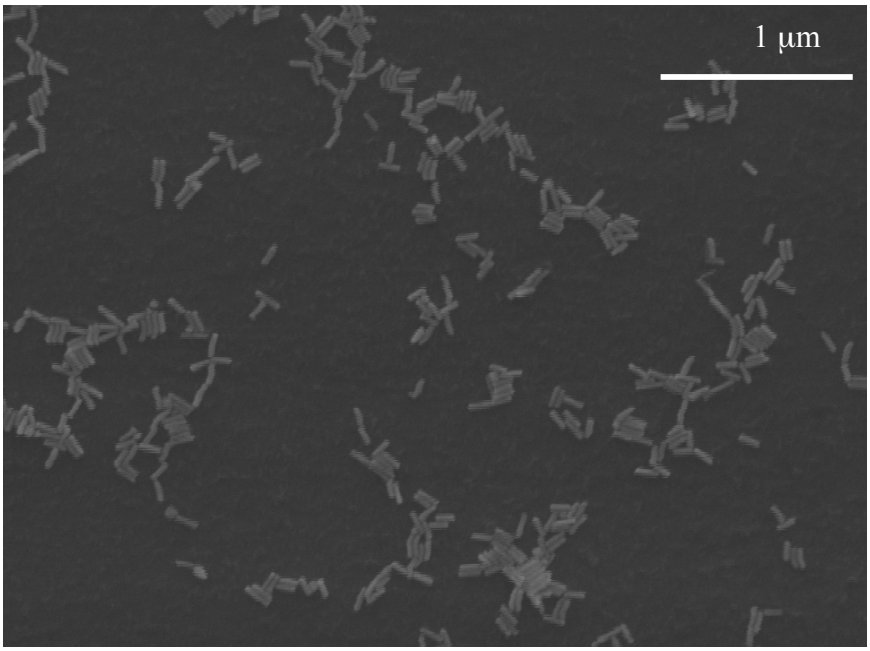

Figure 31: PEG-SH nanorods which have been dispersed in chloroform prior to the removal of excess PEG-SH.

4.3.2 Non-PEGylated Rods:

Addition of nanorods to the Langmuir–Blodgett that were not already functionalized with mPEG-SH was also attempted. In this case, bulk nanorods were rinsed only once and 6.6 μL of chloroform was added to the recovered rinsed product. It was noted in this case that some of the rods had aggregated in the centrifuge tube. This aggregate was removed prior to deposition at the air water interface.

Chloroform was added to the colloidal nanorods and a resultant 20 μL solution was obtained. The entire 20 μL solution was added dropwise to the Langmuir trough. This addition of the nanorods to the air-water interface did not produce any change in the surface pressure. During the compression of the trough barriers the surface pressure did not increase and the experiment was considered a failure. The compression was immediately repeated by changing the target surface pressure to a lower value in the hope that

compression of the barriers to a lower surface pressure might yield some results. However, there was no surface pressure change noted and the experiment was terminated with manual removal of the substrate. The corresponding SEM images resulting from this experiment can be seen in Figure 32 - Figure 35.

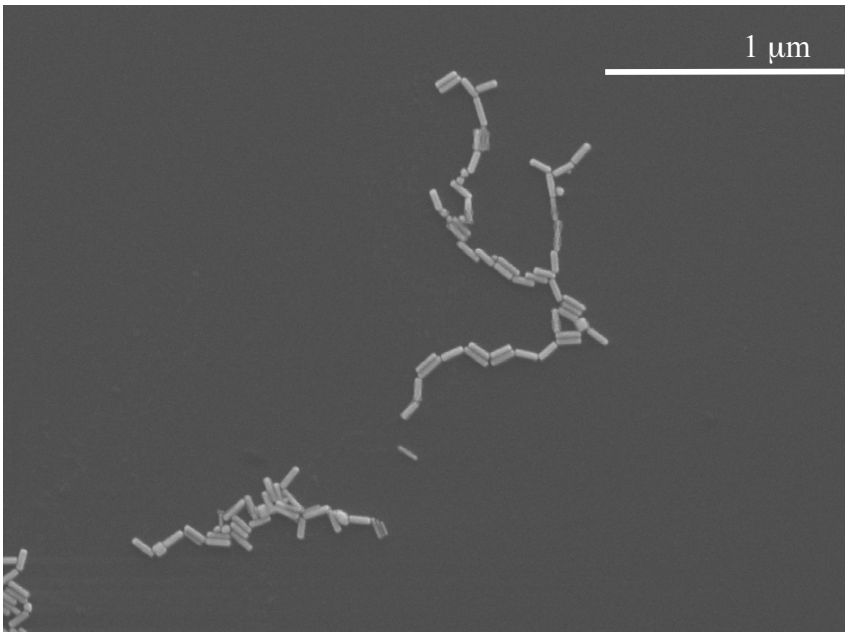

Figure 32: Langmuir-Blodgett deposition of PEGylated gold nanorods dispersed in chloroform, manual electrode removal.

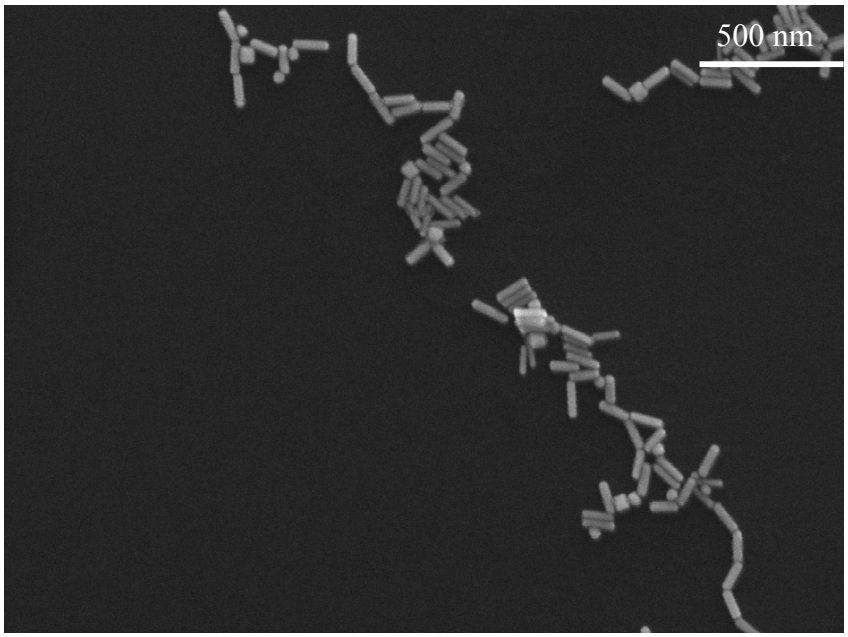

Figure 33: Langmuir-Blodgett deposition of PEGylated gold nanorods dispersed in chloroform, manual electrode removal.

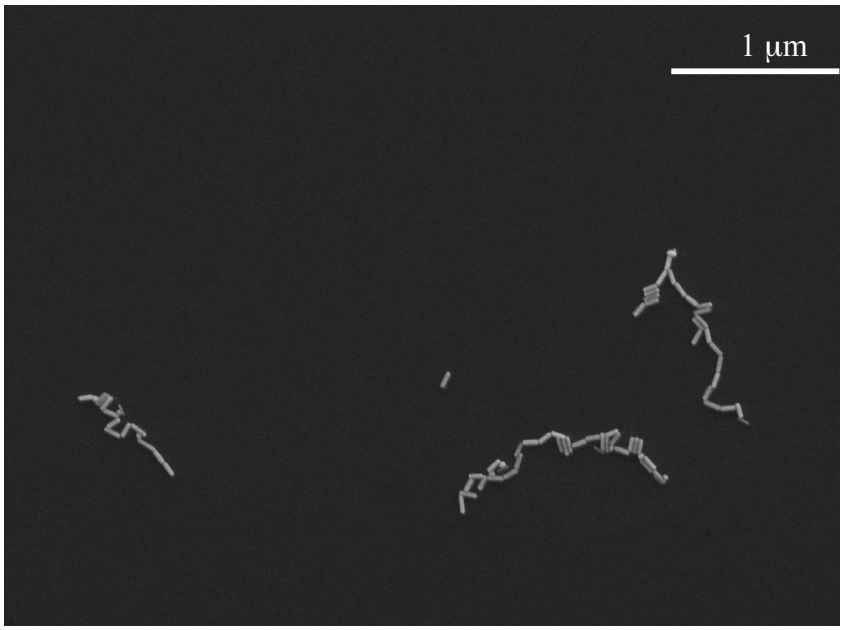

Figure 34: Langmuir-Blodgett deposition of PEGylated gold nanorods dispersed in chloroform, manual electrode removal.

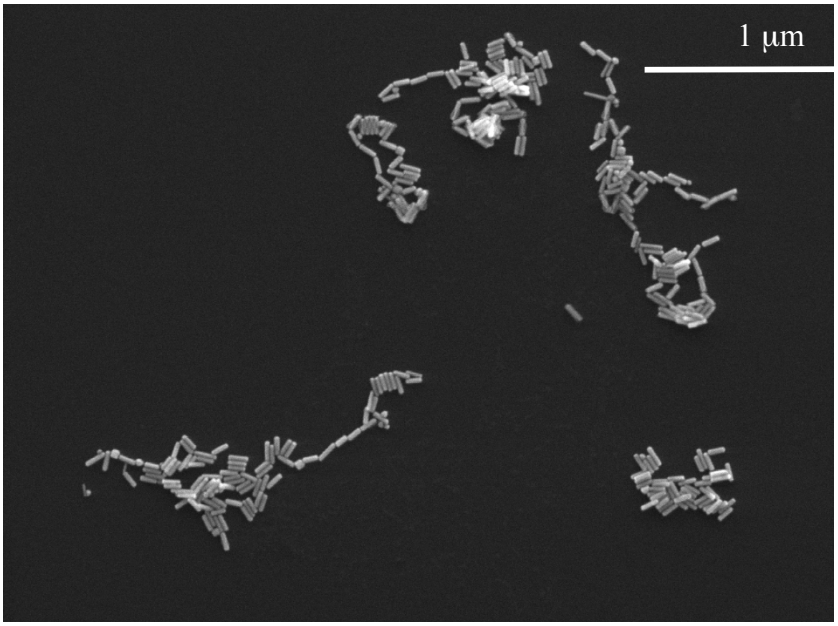

Figure 35: Langmuir-Blodgett deposition of PEGylated gold nanorods dispersed in chloroform, manual electrode removal.

4.3.3 Deposition of PEGylated nanorods in minimal chloroform:

To 100 mL of bulk mPEG-SH nanorods 6.6 μL of chloroform was added. Approximately 8 μL of this nanorod solution was then added dropwise to the air water interface until the surface pressure increased to 1 mN/m. The barriers were compressed at a forward rate of 5 mm/min until the surface pressure increased to 8 mN/m. The transfer ratio for the deposition was 1.811.

This transfer was extremely successful as is shown below in the yielded SEM images in Figure 36 - Figure 38. While a uniform monolayer was not obtained on this substrate, these images indicate that it is at least possible to transfer nanorods to a solid substrate using the Langmuir - Blodgett technique. Evidently in Figure 36 and Figure 37 the rods have orientated in a spherical manner on the substrate. This is referred to as the coffee ring effect.[97,98] To a degree this results from water droplets remaining on the surface of the substrate after its removal from the sub-phase of the Langmuir trough. One can see clearly in Figure 38 that the coffee ring effect does have an impact on the entire substrate. Upon closer inspection of the substrate (as shown in Figure 37), it can be observed that the rods have roughly oriented themselves relative to one another in an end to end, and side to side fashion. This indicates that it is possible to order the nanorods at the air water interface, and to deposit a single layer.

Analysis of Figure 38 highlights the fact that the rods have started to order themselves relative to one another while also showing that the occasional multilayer was formed. This could have been a result of aggregates starting to form at the air-water interface. It should also be noted that the substrate contains no spheres or nanoparticles. This indicated that if the spherical impurities are present in the yielded colloid they do not

transfer to the air-water interface of the Langmuir-Blodgett. It was determined after analyzing these images that transferring PEGylated nanorods to the air water interface was most successful when using the method outlined in Figure 38. In the subsequent sections this method is further optimized to increase surface coverage.

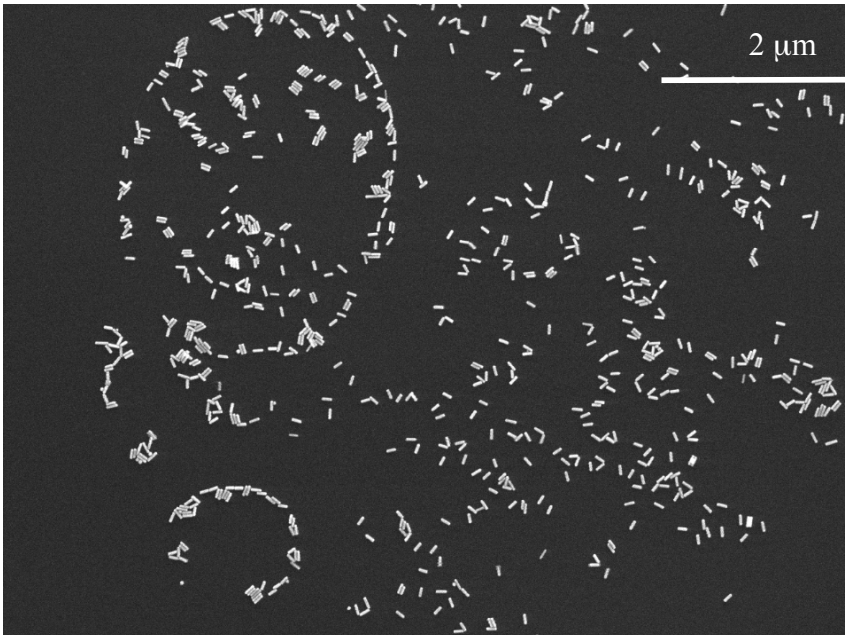

Figure 36: SEM image of Langmuir-Blodgett transfer 100 mL of bulk mPEG-SH colloid dispersed in 6.6 μL chloroform. Close up image showing a coffee ring.

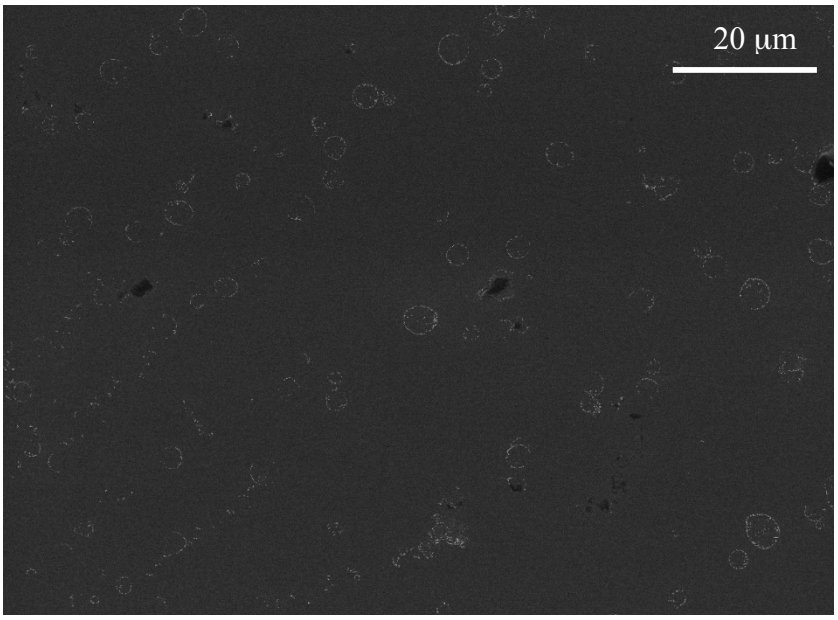

Figure 37: SEM image of Langmuir-Blodgett transfer 100 mL of bulk mPEG-SH colloid dispersed in 6.6 μL chloroform. Show's the coffee ring effect from a distance.

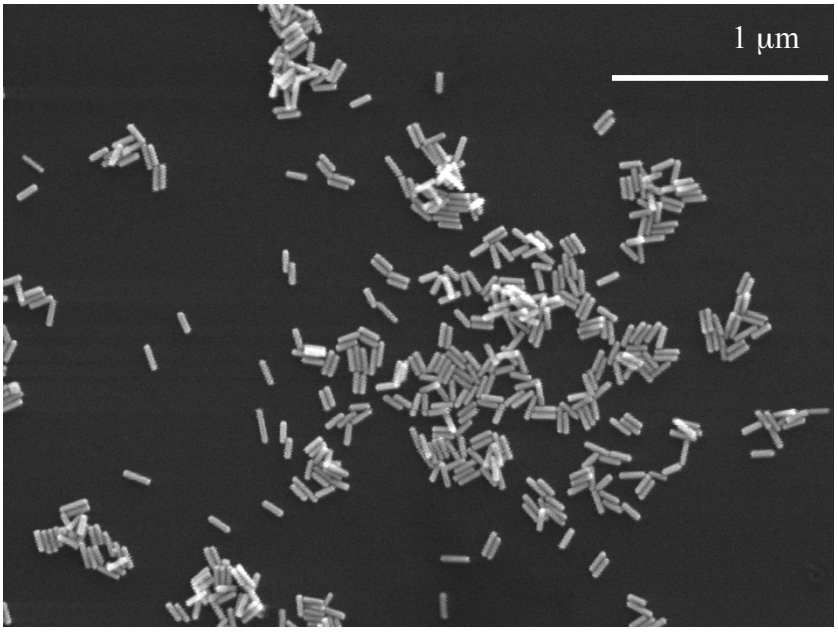

Figure 38: SEM image of Langmuir-Blodgett transfer; 100 mL of bulk mPEG-SH colloid dispersed in 6.6 μL chloroform, showing some multilayer formation.

4.3.4: Optimizing Langmuir – Blodgett Transfers:

To increase coverage of the substrate during the Langmuir-Blodgett transfer the conditions described above were slightly altered and results monitored. 40 μL of the PEGylated colloidal nanorods was dispersed in 6.6 μL of chloroform. Note this is approximately 30 μL more solution than was added in the previous section. The chloroform was allowed to evaporate for 30 minutes in a high humidity environment (90% relative humidity). Prior to the start of the experiment the surface pressure balance was zeroed. Experimentally a target surface pressure increase of 1 mN/m was set as the goal. The trough barriers were minimally compressed when this goal was reached moving only 0.52 mm. The Substrate was then removed automatically yielding a transfer ratio of 0.988. SEM images obtained for this substrate can be seen in Figure 39 -Figure 41. These images highlight the successful increase in surface coverage of the silicon substrate. It is important to note when analyzing these images that a monolayer of nanorods was successfully transferred to the substrate with only a minimal amount of multilayer formation which is visible in Figure 40.

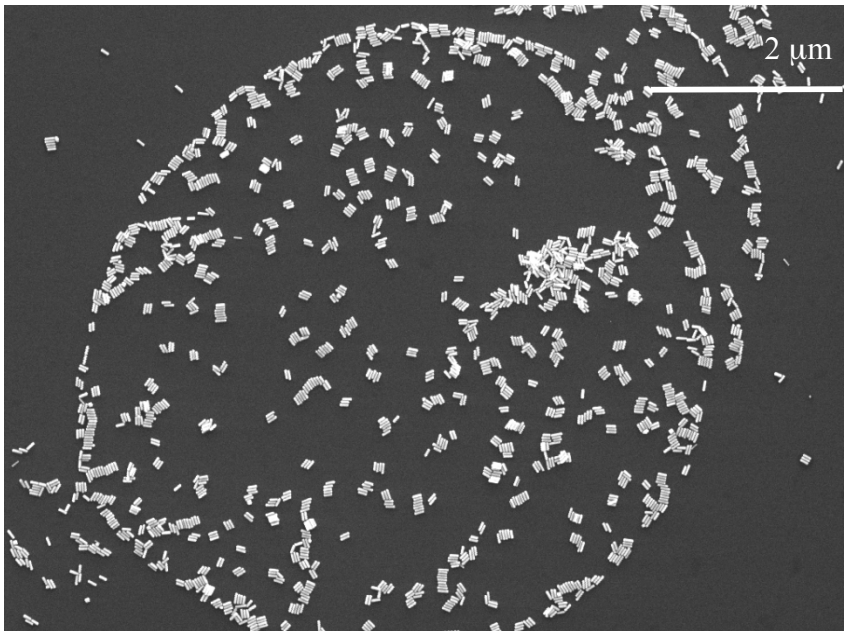

Figure 39: Optimizing the Langmuir-Blodgett transfer of PEGylated colloidal gold nanorods.

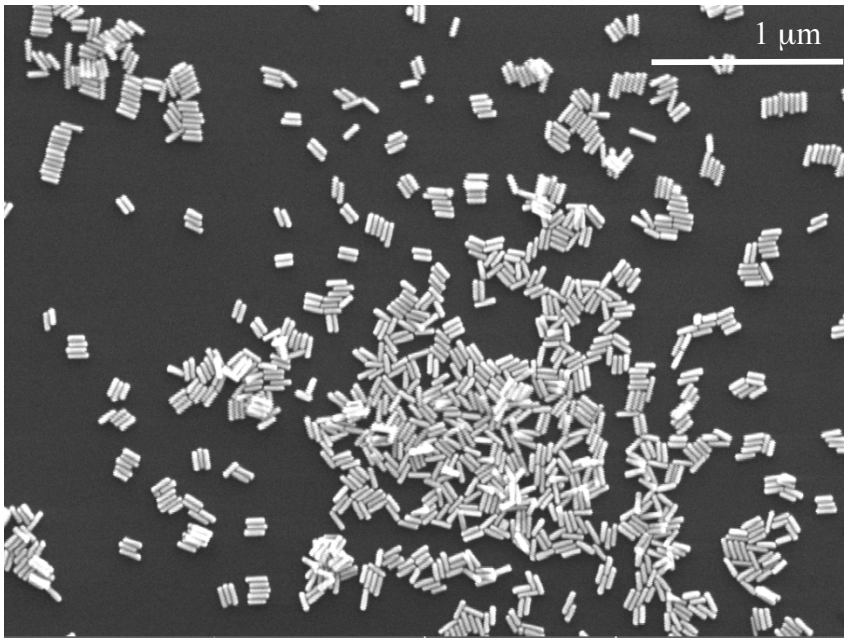

Figure 40: Optimization of the Langmuir-Blodgett transfer of PEGylated colloidal gold nanorods.

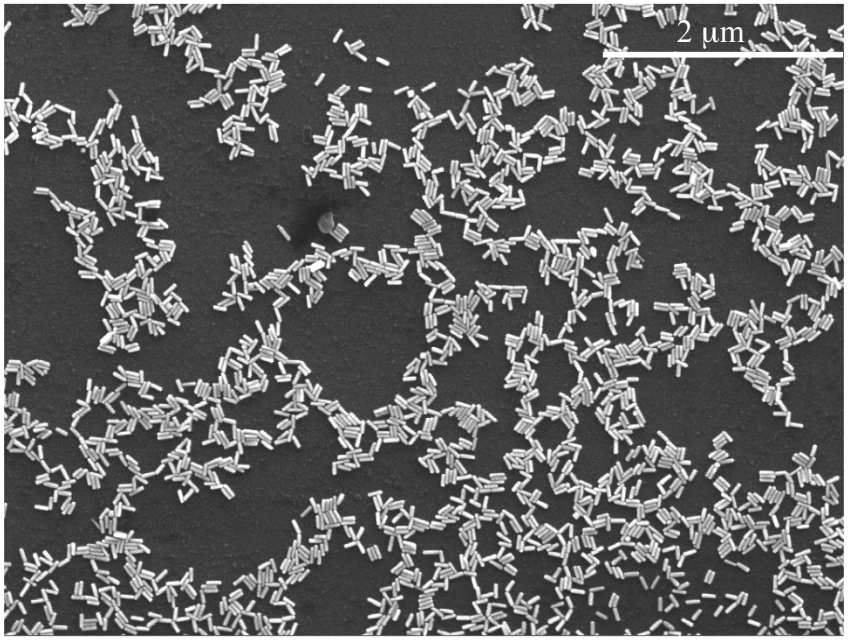

Figure 41: Optimizing the Langmuir-Blodgett transfer of PEGylated colloidal gold nanorods, image showing successful increase of surface coverage.

4.3.5: LSPR sensor analysis:

Using the glass LSPR chips prepared as described above, the two methods (nanorod drop-coat and nanorod incubation) were compared. The comparison of the two methods is best observed by comparing SEM images of the chips. Figure 42Figure 44 show the surface of each of the produced LSPR chips. Based on these images it is clear that the incubated chip highlighted in Figure 44 is more mono-dispersed than that produced using the drop coating method. However, the rods are less densely packed.

Attempts were made to analyze the produced LSPR chips using the Ocean Optics 2000+ spectrophotometer, however no signal was observed due to an instrument malfunction. An example spectrum highlighting the malfunction is shown below in

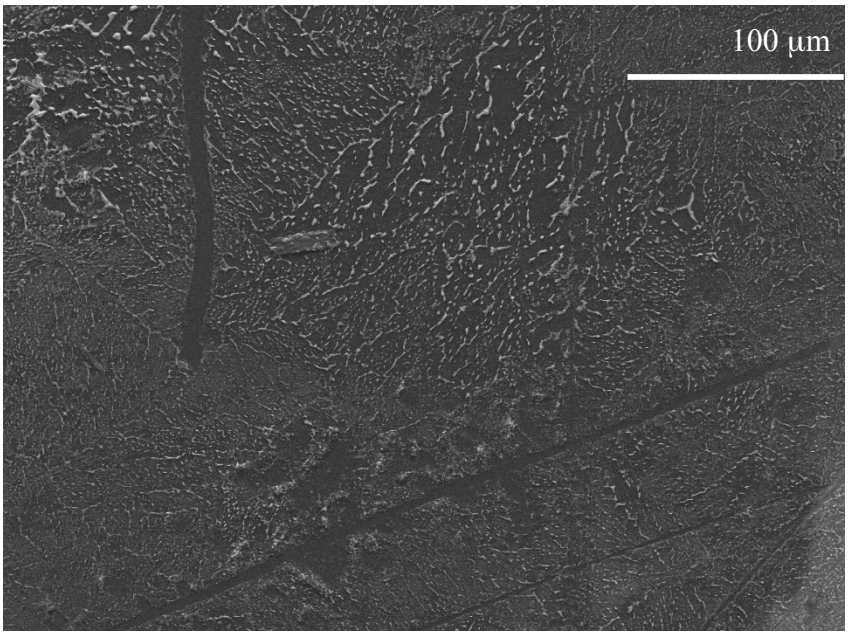

Figure 42: SEM image of the nanorod drop coated LSPR chip.

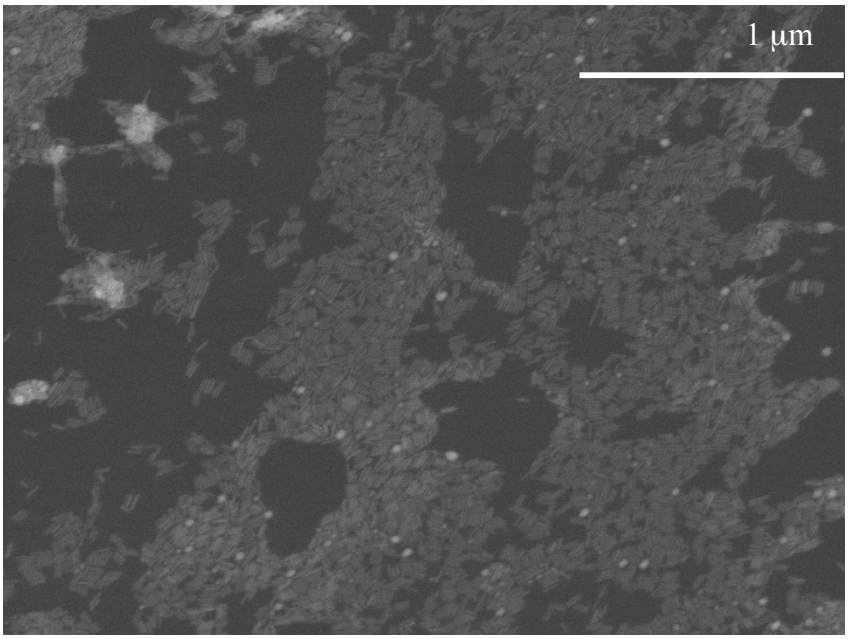

Figure 43: SEM image of the nanorod drop coated LSPR chip at increased magnification.

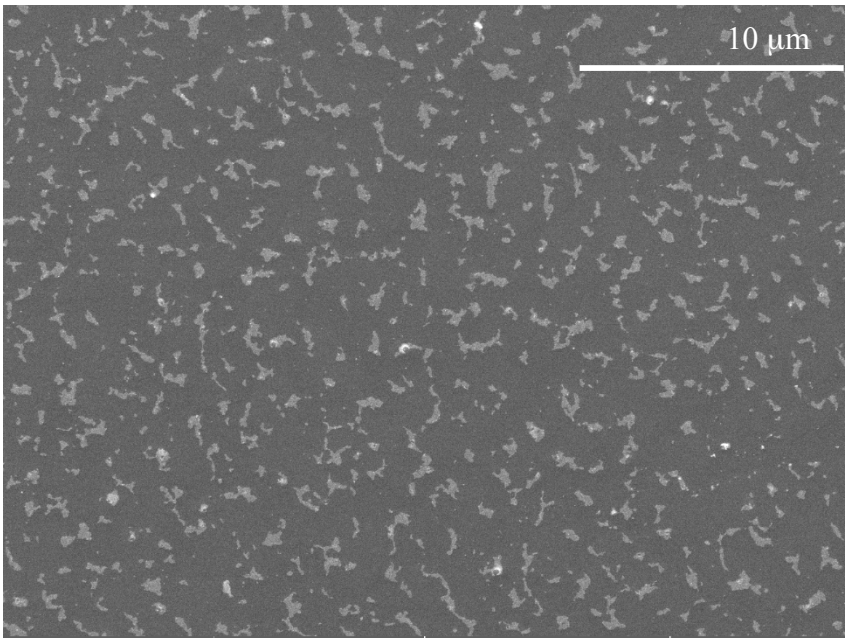

Figure 44: SEM image of the nanorod incubated LSPR chip.

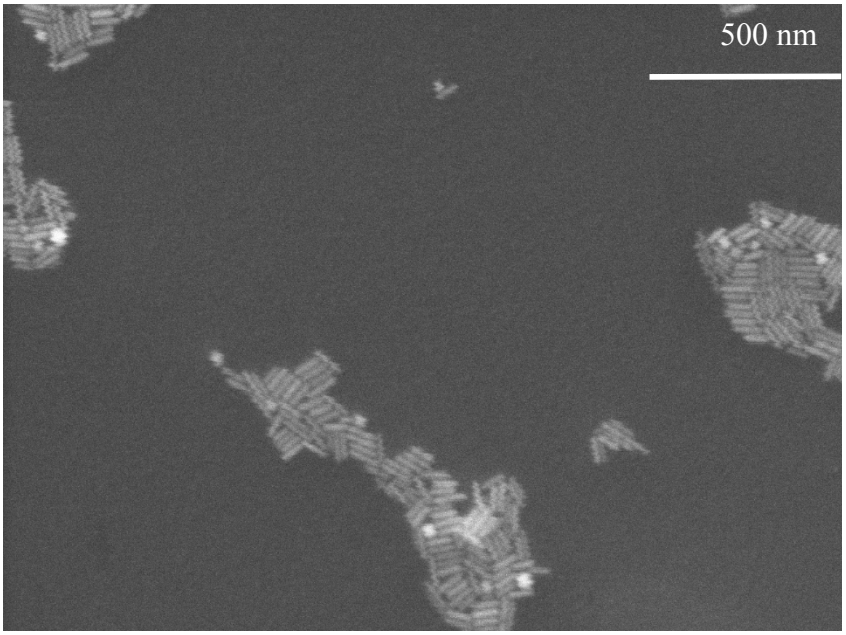

Figure 45: SEM image of the nanorod incubated LSPR chip at increased magnification.

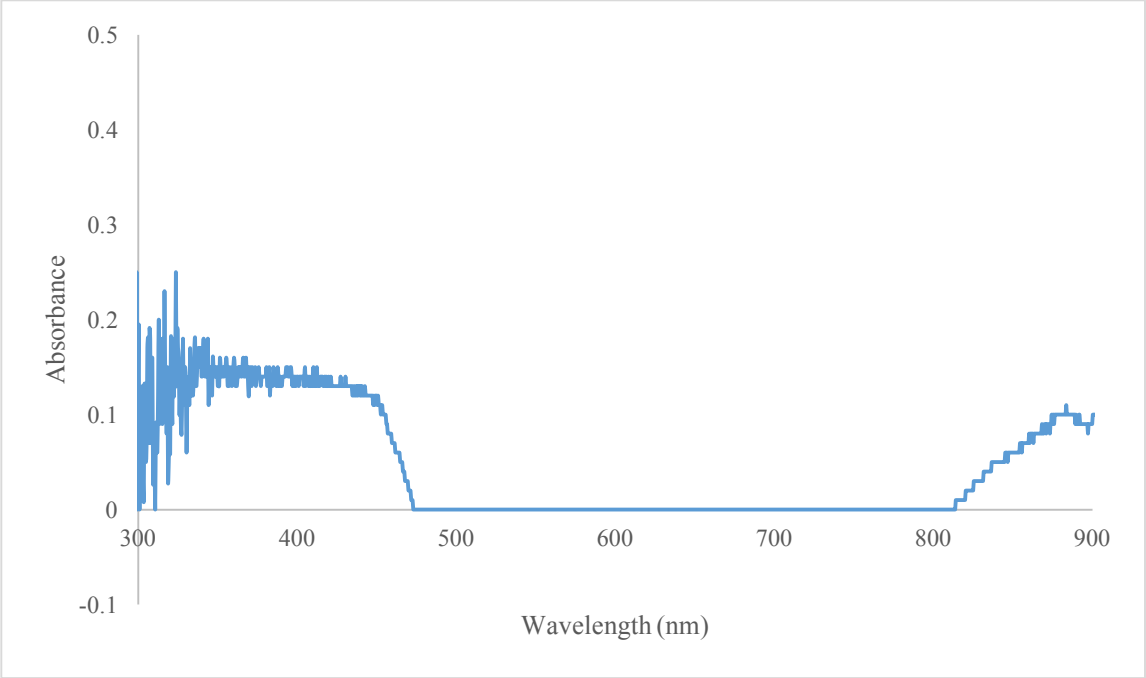

Figure 46: Example absorbance spectrum obtained for LSPR chip highlighting the instrument malfunctions.

Chapter 5: Conclusion and Future Work

Gold nanorods feature tunable LSPR wavelengths making them a useful candidate for various sensing applications. This research was aimed towards providing a proof of concept for the development of an LSPR sensing platform using the Langmuir-Blodgett technique for applying a uniform monolayer of gold nanorods to a solid substrate. It was able to demonstrate that the successful transfer of a monolayer of gold nanorods using the Langmuir-Blodgett method is possible. This transfer was further optimized by functionalizing the synthesized gold nanorod colloid with mPEG-SH, while dispersing the rods in a small amount of chloroform. This research was also able to demonstrate that a mono-dispersed layer of gold nanorods can be transferred to a glass slide following a silanization process with APTMS and the inclusion of an incubation period. This indicates that glass slides functionalized in this manner have the potential to act as sensing platform.

Future work on this project should include introduction of a DNA probe to the glass slide while monitoring changes in the λ_{max} value. A transfer of nanorods to the silanized glass slides should also be attempted using the Langmuir-Blodgett technique with the results then compared to those obtained in this thesis work. Finally, upon completed optimization of these parameters and successful formation of reproducible nanorod monolayers; the transfer of an additional monolayer of nanorods should be attempted for the formation of a multidimensional sensing platform.

Chapter 6: References

1. Canadian Cancer Society Cancer Statistics at a Glance. *http://www.cancer.ca/en/cancer-information/cancer-101/cancer-statistics-at-a-glance/?region=on* (accessed December 5th, 2016).

2. Canadian Cancer Society's Advisory Committee on Cancer Statistics *Canadian Cancer Statistics 2016 - Special Topic;* Canadian Cancer Society: 2016; , pp 142.

3. Manabu Yasui; Yuki Kanemaru; Nagisa Kamoshita; Tetsuya Suzuki; Toshiya Arakawa; Masamitsu Honma Tracing the fates of site-specifically introduced DNA adducts in the human genome. *DNA repair* **2014**, *15*, 11-20.

4. Valavanidis, A.; Vlachogianni, T.; Fiotakis, K.; Loridas, S. Pulmonary Oxidative Stress, Inflammation and Cancer: Respirable Particulate Matter, Fibrous Dusts and Ozone as Major Causes of Lung Carcinogenesis through Reactive Oxygen Species Mechanisms. *International Journal of Environmental Research and Public Health* **2013**, *10*, 3886-3907.

5. Cancer Research, U. K. Waiting times for tests and treatment after cancer diagnosis *http://www.cancerresearchuk.org/about-cancer/cancers-in-general/cancer-questions/waiting-times-for-tests-and-treatment-after-cancer-diagnosis* (accessed December 5th 2016)

6. Petryayeva, E.; Krull, U. Localized surface plasmon resonance: Nanostructures, bioassays and biosensing—A review. *Anal. Chim. Acta* **2011**, *706*, 8-24.

7. Nylander, C.; Liedberg, B.; Lind, T. Gas detection by means of surface plasmon resonance. *Sensors and Actuators* **1982**, *3*, 79-88.

8. Liedberg, B.; Nylander, C.; Lunström, I. Surface plasmon resonance for gas detection and biosensing. *Sensors and Actuators* **1983**, *4*, 299-304.

9. E. Kretschmann; H. Raether Notizen: Radiative Decay of Non Radiative Surface Plasmons Excited by Light. *Zeitschrift für Naturforschung A* **1968**, *23*, 2135-2136.

10. Otto, A. Excitation of nonradiative surface plasma waves in silver by the method of frustrated total reflection. *Zeitschrift für Physik* **1968**, *216*, 398-410.

11. Tang, Y.; Zeng, X.; Liang, J. Surface Plasmon Resonance: An Introduction to a Surface Spectroscopy Technique. *J. Chem. Educ.* **2010**, *87*, 742-746.

12. Yeshchenko, O. A.; Bondarchuk, I. S.; Gurin, V. S.; Dmitruk, I. M.; Kotko, A. V. Temperature dependence of the surface plasmon resonance in gold nanoparticles. *Surf. Sci.* **2013***, 608*, 275-281.

13. Stuart, D. A. Biological applications of localised surface plasmonic phenomenae. *IEE Proceedings - Nanobiotechnology* **2005***, 152*, 13-32.

14. Jung, L. S.; Campbell, C. T.; Chinowsky, T. M.; Mar, M. N.; Yee, S. S. Quantitative Interpretation of the Response of Surface Plasmon Resonance Sensors to Adsorbed Films. *Langmuir* **1998***, 14*, 5636-5648.

15. Malinsky, M. D.; Kelly, K. L.; Schatz, G. C.; Van Duyne, R. P. Chain Length Dependence and Sensing Capabilities of the Localized Surface Plasmon Resonance of Silver Nanoparticles Chemically Modified with Alkanethiol Self-Assembled Monolayers. *J. Am. Chem. Soc.* **2001***, 123*, 1471-1482.

16. Sabban, S. Development of an in vitro model system for studying the interaction of Equus caballus lgE with its high-affinity Fc receptor, The University of Sheffield, 2011.

17. Hammond, J. L.; Bhalla, N.; Rafiee, S. D.; Estrela, P. Localized Surface Plasmon Resonance as a Biosensing Platform for Developing Countries. *Biosensors* **2014***, 4*, 172-188.

18. Willets, K. Localized surface plasmon resonance spectroscopy and sensing. *Annu. Rev. Phys. Chem.* **2007***, 58*, 267-97.

19. Miller, M. M.; Lazarides, A. A. Sensitivity of Metal Nanoparticle Surface Plasmon Resonance to the Dielectric Environment. *J Phys Chem B* **2005***, 109*, 21556-21565.

20. Miller, M.; Lazarides, A. Sensitivity of metal nanoparticle plasmon resonance band position to the dielectric environment as observed in scattering. *Journal of optics.A, Pure and applied optics* **2006***, 8*, S249.

21. Aćimović, S. S.; Kreuzer, M. P.; Quidant, R. Engineering Through Mode Shaping and Lithographical Nanofabrication of Ultrasensitive Nano-plasmonic Sensors for Molecular Detection. In *Nanoplasmonic Sensors*; Dmitriev, A., Ed.; Springer New York: New York, NY, 2012; pp 267-287.

22. Heiligtag, F. J.; Niederberger, M. The fascinating world of nanoparticle research. *Materials Today* **2013***, 16*, 262-271.

23. Royal Institution Michael Faraday's gold colloids. *http://www.rigb.org/our-history/iconic-objects/iconic-objects-list/faraday-gold-colloids* (accessed December 7th 2016)

24. Huang, X.; El-Sayed, M. A. Gold nanoparticles: Optical properties and implementations in cancer diagnosis and photothermal therapy. *Journal of Advanced Research* **2010***, 1*, 13-28.

25. Sajanlal, P. R.; Sreeprasad, T. S.; Samal, A. K.; Pradeep, T. Anisotropic nanomaterials: structure, growth, assembly, and functions. *Nano Reviews* **2010***, 2*, 10.3402/nano.v2i0.5883.

26. Ankamwar, B. Size and Shape Effect on Biomedical Applications of Nanomaterials. In 2012; .

27. Albanese, A.; Tang, P. S.; Chan, W. C. W. The Effect of Nanoparticle Size, Shape, and Surface Chemistry on Biological Systems. *Annual Review of Biomedical Engineering* **2012***, 14*, 1-16.

28. Tong, L.; Wei, Q.; Wei, A.; Cheng, J. Gold nanorods as contrast agents for biological imaging: optical properties, surface conjugation, and photothermal effects. *Photochem. Photobiol.* **2009***, 85*, 21.

29. Nikoobakht, B.; El-Sayed, M. Preparation and Growth Mechanism of Gold Nanorods (NRs) Using Seed-Mediated Growth Method. *Chem. Mater.* **2003***, 15*, 1957-1962.

30. Gole, A.; Murphy, C. J. Seed-Mediated Synthesis of Gold Nanorods: Role of the Size and Nature of the Seed. *Chem. Mater.* **2004***, 16*, 3633-3640.

31. Pérez-Juste, J.; Pastoriza-Santos, I.; Liz-Marzán, L. M.; Mulvaney, P. Gold nanorods: Synthesis, characterization and applications. *Coord. Chem. Rev.* **2005***, 249*, 1870-1901.

32. Jain, P. K.; Huang, X.; El-Sayed, I. H.; El-Sayed, M. A. Noble metals on the nanoscale: optical and photothermal properties and some applications in imaging, sensing, biology, and medicine. *Accounts of chemical research* **2008***, 41*, 1578-1586.

33. Dreaden, E. C.; Alkilany, A. M.; Huang, X.; Murphy, C. J.; El-Sayed, M. A. The golden age: gold nanoparticles for biomedicine. *Chemical Society reviews* **2012***, 41*, 2740-2779.

34. Eustis, S.; El-Sayed, M. A. Why gold nanoparticles are more precious than pretty gold: Noble metal surface plasmon resonance and its enhancement of the radiative and nonradiative properties of nanocrystals of different shapes. *Chemical Society Reviews* **2006***, 35*, 29-217.

35. Burda, C.; Chen, X.; Narayanan, R.; El-Sayed, M. A. Chemistry and properties of nanocrystals of different shapes. *Chemical reviews* **2005***, 105*, 1025-1102.

36. Murphy, C. J.; Gole, A. M.; Hunyadi, S. E.; Orendorff, C. J. One-dimensional colloidal gold and silver nanostructures. *Inorganic chemistry* **2006***, 45*, 7544-7554.

37. Lohse, S. E.; Murphy, C. J. The Quest for Shape Control: A History of Gold Nanorod Synthesis. *Chem. Mater.* **2013***, 25*, 1250-1261.

38. Jain, P. K.; Lee, K. S.; El-Sayed, I.; El-Sayed, M. Calculated Absorption and Scattering Properties of Gold Nanoparticles of Different Size, Shape, and Composition: Applications in Biological Imaging and Biomedicine. *J Phys Chem B* **2006***, 110*, 7238-7248.

39. Ali, M. R. K.; Snyder, B.; El-Sayed, M. Synthesis and Optical Properties of Small Au Nanorods Using a Seedless Growth Technique. *Langmuir* **2012***, 28*, 9807-9815.

40. Orendorff, C. J.; Murphy, C. J. Quantitation of Metal Content in the Silver-Assisted Growth of Gold Nanorods. *J Phys Chem B* **2006***, 110*, 3990-3994.

41. Ni, W.; Kou, X.; Yang, Z.; Wang, J. Tailoring Longitudinal Surface Plasmon Wavelengths, Scattering and Absorption Cross Sections of Gold Nanorods. *ACS Nano* **2008***, 2*, 677-686.

42. Prescott, S. W.; Mulvaney, P. Gold nanorod extinction spectra. *J. Appl. Phys.* **2006***, 99*, 123504.

43. Link, S.; El-Sayed, M. Spectral Properties and Relaxation Dynamics of Surface Plasmon Electronic Oscillations in Gold and Silver Nanodots and Nanorods. *J Phys Chem B* **1999***, 103*, 8410-8426.

44. Si, S.; Leduc, C.; Delville, M.; Lounis, B. Short Gold Nanorod Growth Revisited: The Critical Role of the Bromide Counterion. *ChemPhysChem* **2012***, 13*, 193-202.

45. Huang, X.; Neretina, S.; El-Sayed, M. A. Gold Nanorods: From Synthesis and Properties to Biological and Biomedical Applications. *Adv Mater* **2009***, 21*, 4880-4910.

46. Stewart, M. E.; Anderton, C. R.; Thompson, L. B.; Maria, J.; Gray, S. K.; Rogers, J. A.; Nuzzo, R. G. Nanostructured plasmonic sensors. *Chemical reviews* **2008***, 108*, 494-521.

47. Seshadri, S. R. Attenuated total reflection method of excitation of the surface polariton in the Kretschmann configuration. *Journal of Applied Physics* **1991***, 70*, 3647-3654.

48. Junxue Fu; Bosoon Park; Yiping Zhao Nanorod-mediated surface plasmon resonance sensor based on effective medium theory. *Applied Optics* **2009***, 48*, 4637-4649.

49. Soon Joon Yoon; Donghyun Kim Target dependence of the sensitivity in periodic nanowire-based localized surface plasmon resonance biosensors. *Journal of the Optical Society of America A* **2008**, *25*, 725-735.

50. Xiaoyan Yang; Deming Liu Sensitivity enhancement of surface plasmon resonance sensors through planar metallic film closely coupled to nanogratings. *Chinese Optics Letters* **2007**, *5*, 563-565.

51. Fainman, Y.; Hwang, G.; Slutsky, B.; Pang, L. Spectral sensitivity of two-dimensional nanohole array surface plasmon polariton resonance sensor. *Applied Physics Letters* **2007**, *91*, 3.

52. Donghyun Kim Effect of resonant localized plasmon coupling on the sensitivity enhancement of nanowire-based surface plasmon resonance biosensors. *Journal of the Optical Society of America A* **2006**, *23*, 2307-2314.

53. Gu, J. H.; Lü, H.; Chen, Y. W.; Liu, L. Y.; Wang, P.; Ma, J. M.; Lu, Z. H. Enhancement of the sensitivity of surface plasmon resonance biosensor with colloidal gold labeling technique. *Supramolecular Science* **1998**, *5*, 695-698.

54. Kyung Min Byun; Soon Joon Yoon; Donghyun Kim; Sung June Kim Sensitivity analysis of a nanowire-based surface plasmon resonance biosensor in the presence of surface roughness. *Journal of the Optical Society of America A* **2007**, *24*, 522-529.

55. Kyung Min Byun; Soon Joon Yoon; Donghyun Kim; Sung June Kim Experimental study of sensitivity enhancement in surface plasmon resonance biosensors by use of periodic metallic nanowires. *Optics Letters* **2007**, *32*, 1902-1904.

56. Byun, K. M.; Kim, S. J.; Kim, D. Investigation of the profile effect on the sensitivity enhancement of nanowire-mediated localized surface plasmon resonance biosensors. *Sensors & Actuators: B. Chemical* **2006**, *117*, 401-407.

57. Cao, J.; Sun, T.; Grattan, K. T. V. Gold nanorod-based localized surface plasmon resonance biosensors: A review. *Sensors and Actuators B: Chemical* **2014**, *195*, 332-351.

58. Rayleigh Surface Tension. *Nature* **1891**, *43*, 437-439.

59. Hussain, S. A. Langmuir-Blodgett Films a unique tool for molecular electronics. **2009**.

60. KSV NIMA What and why: Langmuir-Blodgett films. *http://www.biolinscientific.com/zafepress.php?url=%2Fpdf%2FKSV%20NIMA%2FTheory%20Notes%2FKN_TN_1_what-and-why-langmuir-films.pdf* (accessed Feb 25, 2017).

61. Kim, F.; Kwan, S.; Akana, J.; Yang, P. Langmuir−Blodgett Nanorod Assembly. *J. Am. Chem. Soc.* **2001***, 123*, 4360-4361.

62. Kinge, S.; Crego-Calama, M.; Reinhoudt, D. N. Self-Assembling Nanoparticles at Surfaces and Interfaces. *ChemPhysChem* **2008***, 9*, 20-42.

63. Shipway, A. N.; Katz, E.; Willner, I. Nanoparticle arrays on surfaces for electronic, optical, and sensor applications. *Chemphyschem : a European journal of chemical physics and physical chemistry* **2000***, 1*, 18.

64. Deák, A.; Bancsi, B.; Tóth, A. L.; Kovács, A. L.; Hórvölgyi, Z. Complex Langmuir–Blodgett films from silica nanoparticles: An optical spectroscopy study. *Colloids Surf. Physicochem. Eng. Aspects* **2006***, 278*, 10-16.

65. Genson, K. L.; Holzmueller, J.; Jiang, C.; Xu, J.; Gibson, J. D.; Zubarev, E. R.; Tsukruk, V. V. Langmuir−Blodgett Monolayers of Gold Nanoparticles with Amphiphilic Shells from V-Shaped Binary Polymer Arms. *Langmuir* **2006***, 22*, 7011-7015.

66. Li, W.; Xu, R.; Wang, L.; Cui, H.; Xi, S. Superlattice Structure of Gold Nanoparticles Film Deposited by Langmuir-Blodgett Technique. *Molecular Crystals and Liquid Crystals Science and Technology. Section A. Molecular Crystals and Liquid Crystals* **1999***, 337*, 185-188.

67. Zhou, W.; Odom, T. W. Tunable subradiant lattice plasmons by out-of-plane dipolar interactions. *Nat Nano* **2011***, 6*, 423-427.

68. Kim, Y.; Na, H.; Ham, S.; Min, D. Mediating ordered assembly of gold nanorods by controlling droplet evaporation modes for surface enhanced Raman scattering. *RSC Adv.* **2014***, 4*, 50091-50096.

69. Petty, M. C. *Langmuir-Blodgett Films - An Introduction;* Cambridge University Press: Cambridge, 1996; .

70. Shaw, D. J. Introduction to Colloid and Surface Chemistry. In *Introduction to Colloid and Surface Chemistry (Fourth Edition)*Butterworth-Heinemann: Oxford, 1992; pp 64-114.

71. Furbish, D. *Fluid physics in geology : an introduction to fluid motions on Earth's surface and within its crust;* Oxford University Press: New York, 1997; .

72. Mingins, J.; Pethica, B. A. Intermolecular Forces in Spread Phospholipid Monolayers at Oil/Water Interfaces. *Langmuir* **2004***, 20*, 7493-7498.

73. Karaballi, R. Spectroscopic investigation of the interaction between biomimetic membranes and protein aggregates, Saint Mary's University, 2015.

74. Barnes, G.; Gentle, I. *Interfacial Science: An Introduction;* OUP Oxford: 2011; .

75. Yang, P.; Kim, F. Langmuir-Blodgett assembly of one-dimensional nanostructures. *Chemphyschem : a European journal of chemical physics and physical chemistry* **2002**, *3*, 503.

76. Zhou, W.; Wang, Z. *Scanning Microscopy for Nanotechnology;* Springer-Verlag: 2007; .

77. Schweitzer, J. Scanning Electron Microscope. https://www.purdue.edu/ehps/rem/rs/sem.htm (accessed September 2nd 2016)

78. Wilson, S. M.; Bacic, A. Preparation of plant cells for transmission electron microscopy to optimize immunogold labeling of carbohydrate and protein epitopes. *Nat. Protocols* **2012**, *7*, 1716-1727.

79. Goldstein, J. I.; Newbury, D. E.; Echlin, P.; Joy, D. C.; Lyman, C. E.; Lifshin, E.; Michael, J. R.; Romig Jr., A. D.; Fiori, C. *Scanning Electron Microscopy and X-ray Microanalysis;* Springer US: Boston, MA, 1992; , pp 1-10.

80. Goldstein, J.; Newbury, D.; Echlin, P.; Joy, D.; Lyman, C.; Lifshin, E.; Sawyer, L.; Michael, J. *Scanning Electron Microscopy and X-ray Microanalysis;* Springer US: Boston, MA, 2003; , pp 1-10.

81. Khursheed, A. *Scanning electron microscope optics and spectrometers;* World Scientific Pub Co Pte: London, 2011; .

82. Reimer, L. Transmission Electron Microscopy.

83. Egerton, R. F. *Physical Principles of Electron Microscopy : An Introduction to TEM, SEM, and AEM;* Springer: Boston, MA, 2005; .

84. nanoComposix UV/VIS/IR SPECTROSCOPY ANALYSIS OF NANOPARTICLES http://50.87.149.212/sites/default/files/nanoComposix%20Guidelines%20for%20UV-vis%20Analysis.pdf. (accessed April 8th 2017)

85. Jana, N. R.; Gearheart, L.; Murphy, C. J. Wet chemical synthesis of silver nanorods and nanowires of controllable aspect ratio. *Chemical Communications* **2001**, 617-618.

86. Jiang XC, Pileni MP. Gold nanorods: Influence of various parameters as seeds, solvent, surfactant on shape control. *Colloids Surf Physicochem Eng Aspects*. 2007;295(1–3):228-232.

87. Ye, X.; Zheng, C.; Chen, J.; Gao, Y.; Murray, C. B. Using Binary Surfactant Mixtures To Simultaneously Improve the Dimensional Tunability and Monodispersity in the Seeded Growth of Gold Nanorods. *Nano Lett.* **2013***, 13*, 765-771.

88. Khlebtsov, B. N.; Khanadeev, V. A.; Ye, J.; Sukhorukov, G. B.; Khlebtsov, N. G. Overgrowth of Gold Nanorods by Using a Binary Surfactant Mixture. *Langmuir* **2014***, 30*, 1696-1703.

89. Guo, Z.; Fan, X.; Xu, L.; Lu, X.; Gu, C.; Bian, Z.; Gu, N.; Zhang, J.; Yang, D. Shape separation of colloidal gold nanoparticles through salt-triggered selective precipitation. *Chem. Commun.* **2011***, 47*, 4180-4182.

90. Mahmoud, M. A. Controlling the orientations of gold nanorods inside highly packed 2D arrays. *Physical chemistry chemical physics : PCCP* **2014***, 16*, 26153-26162.

91. Alkilany, A. M.; Yaseen, A. I. B.; Park, J.; Eller, J. R.; Murphy, C. J. Facile phase transfer of gold nanoparticles from aqueous solution to organic solvents with thiolated poly(ethylene glycol). *RSC Adv* **2014***, 4*, 52676-52679.

92. Li, J.; Zhu, B.; Zhu, Z.; Zhang, Y.; Yao, X.; Tu, S.; Liu, R.; Jia, S.; Yang, C. J. Simple and Rapid Functionalization of Gold Nanorods with Oligonucleotides Using an mPEG-SH/Tween 20-Assisted Approach. *Langmuir* **2015***, 31*, 7869-7876.

93. Rostro-Kohanloo, B. C.; Bickford, L. R.; Payne, C. M.; Day, E. S.; Anderson, L. J. E.; Zhong, M.; Lee, S.; Mayer, K. M.; Zal, T.; Adam, L.; Dinney, C. P. N.; Drezek, R. A.; West, J. L.; Hafner, J. H. The stabilization and targeting of surfactant-synthesized gold nanorods. *Nanotechnology* **2009***, 20*, 434005.

94. Xiaohu Xia; Miaoxin Yang; Yucai Wang; Yiqun Zheng; Qingge Li; Jingyi Chen; Younan Xia Quantifying the coverage density of poly(ethylene glycol) chains on the surface of gold nanostructures. *ACS nano* **2012***, 6*, 512-522.

95. Zhang, Z.; Lin, M. Fast loading of PEG–SH on CTAB-protected gold nanorods. *RSC Advances* **2014***, 4*, 17760.

96. Hakkinen, H. The gold-sulfur interface at the nanoscale. *Nat Chem* **2012***, 4*, 443-455.

97. Li, Y.; Zhao, Z.; Lam, M. L.; Liu, W.; Yeung, P. P.; Chieng, C.; Chen, T. Hybridization-induced suppression of coffee ring effect for nucleic acid detection. *Sensors and Actuators B: Chemical* **2015***, 206*, 56-64.

98. Xu, T.; Lam, M. L.; Chen, T. Discrete Element Model for Suppression of Coffee-Ring Effect. *Scientific Reports* **2017***, 7*, 42817.